

NASA-CR-195257

HQROM93.WR1

111-90-CR

**FINAL REPORT**

August 1992 through October 1993

**COLLISIONLESS SHOCK STRUCTURES OF EARTH AND OTHER  
PLANETS**

NASA Contract NASW-4749

November 1993

Principal Investigator: Eugene W. Greenstadt

Co-Investigator: Stewart L. Moses

*Electromagnetic Systems and Technology Department, TRW*

TRW Space and Technology Group  
Applied Technology Division  
One Space Park  
Redondo Beach, CA 90278

(NASA-CR-195257) COLLISIONLESS  
SHOCK STRUCTURES OF EARTH AND OTHER  
PLANETS Final Report, Aug. 1992 -  
Oct. 1993 (TRW Space Technology  
Labs.) 65 p

N94-27407

Unclass

G3 ~~FF~~/90 0210654

# FINAL REPORT

## COLLISIONLESS SHOCK STRUCTURES OF EARTH AND OTHER PLANETS

November, 1993

Principal Investigator: Eugene W. Greenstadt  
Co-Investigator: Stewart L. Moses

### Technical Summary

#### *Introduction*

This report summarizes the closing segment of our multi-spacecraft, multi-instrument study of collisionless shock structure. In this last year of our study, we have necessarily concentrated on subjects that limited time and remaining resources could be expected to bring to reasonable stopping points, if not full conclusions. Our attention has been focused therefore on matters that were either well underway when the year began or that could be expected to yield rapidly completed reports publishable quickly in abbreviated versions. Contemporary publication delays prevent any new initiatives from reaching the literature within the year in the best of circumstances. The topics that fell into these categories were detailed plasma wave (pw) phenomenology in slow shocks in the Earth's distant geomagnetic tail, instantaneous orientations of  $\theta_{Bn}$  in quasiparallel ( $Q_{\parallel}$ ) shock structure, and a comprehensive overview of the relationship between structural ULF waves in the  $Q_{\parallel}$  shock environment and waves in the magnetosphere, i.e. geomagnetic ULF pulsations. The remainder of this report describes our freshly completed results, discusses two related investigations of pw waves in the foreshock and magnetosheath, and appends the abstracts of published papers and the texts of papers in press.

#### *Plasma Waves in Slow Shocks*

The region surrounding Earth's magnetosphere is not the only one where a shock can, and does, exist in Earth's plasma environment. Reconnection sites also have associated shocks, but these are slow shocks. One such site, variable in position, is deep in the geotail and was accessible to measurements by ISEE 3. Although slow shocks were identified in the tail and their average associated plasma wave turbulence was described almost a decade ago, a detailed account of their pw spectra and polarizations had never been developed or

published. We undertook to rectify this deficiency and finally succeeded in this last interval of our investigation in completing a description of the pw behavior of the ramps and up- and downstream regions of the previously discovered slow shocks, with help from another program. The pw activity was bimodal within the ramps, with the higher of the two frequency modes representing a new emission downstream. A paper on this study, by Coroniti has just been completed and submitted for publication; a copy is appended to this report.

### *Instantaneous B Orientation*

$Q_{\parallel}$  shock structure begs certain questions of self consistency. The two most important issues are: First, with no single obvious quasiperpendicular ( $Q_{\perp}$ ) jump step in magnetic and other parameters as the shock is traversed, where, and exactly what, is the  $Q_{\parallel}$  "shock crossing?" Second, how exactly is the instantaneous  $Q_{\parallel}$  or  $Q_{\perp}$  condition defined within a region in which the ambient field is highly variable and the local normal to the elusive "shock" cannot be discerned?

The first question has been essentially answered by observations and numerical simulations. There seems to be a well defined instant in the midst of the turbulent records of most  $Q_{\parallel}$  crossings where the plasma parameters, notably the electron density, undergo a significant change between upstream and downstream values. In fact, we have learned with respectable consistency to identify in the magnetic field profiles the most probable point where the plasma shock occurs. In addition, computer modeling has converged on a picture of the  $Q_{\parallel}$  shock in which its wave and particle components combine to continually "reform" the true "shock crossing" where enlarged ULF wave signals, convected into the shock by the solar wind, have developed gradients of sufficient magnitude to perform the usual functions of the  $Q_{\perp}$  jump transition. The statistical location of Earth's  $Q_{\parallel}$  bow shock crossings has demonstrated clearly that the overriding influence of total energy balance between the solar wind and the magnetosphere determines the approximate site of the "shock" regardless of the local field geometry, and therefore the meaning of a more or less reliable local "normal" based on the general shape of the shock.

The second question was addressed in a preliminary way some years ago by *Greenstadt and Mellott* [1985], who documented the instantaneous oscillation of  $\mathbf{B}$  between  $Q_{\parallel}$  and  $Q_{\perp}$  geometry, with respect to a fixed model normal, caused by the inevitable presence of the ULF waves in the  $Q_{\parallel}$  foreshock. In the development of that study a few instances were displayed in which the  $\theta_{Bn}$  at the actual  $Q_{\parallel}$  crossings corresponded to locally  $Q_{\perp}$  conditions, i.e.,  $\theta_{Bn} > 45^{\circ}$ . Recent simulations by *Scholer and Burgess* [1992] showed that enlargements of upstream waves leading to reformed shock gradients were accompanied, if not triggered, by local excursions of  $\theta_{Bn}$  above the  $Q_{\perp}$  threshold. To follow up our earlier observations and to test these results in the bow shock, we gathered examples of foreshock waves and pulses near the shock and examined their geometric environment. One of our completed studies showed that at least a class of  $Q_{\parallel}$  crossings

and large amplitude upstream pulsations were preceded, perhaps even surrounded, by  $Q_{\perp}$  field, thus validating in nature the participation of  $Q_{\perp}-\theta_{Bn}$  in the simulated shock reformation process. The first page of the published paper on this subject is included in the last section of this report.

### *ULF in the Magnetosphere*

Daytime magnetospheric ULF pulsations have long been linked to solar wind parameters, but the actual machinery by which waves in the magnetosphere are stimulated is still unsettled. A consensus has developed around the inference that pulsations in the range  $.007 < f < .07$  Hz derive in some manner, directly or indirectly from foreshock and bow shock waves and pulsations in the same frequency range. Such external waves contribute to the broadband ULF spectrum in the magnetosheath and propagate to, or distribute themselves around, the daytime magnetopause, penetrating it somewhere, somehow, with enough energy to activate the natural resonances inside. Both theoretical and observational studies have shown that magnetosheath waves can be severely attenuated by the magnetopause; correlations of pulsations against solar wind parameters have been widely scattered and correlations of simultaneous measurements in- and outside the magnetopause have been encouraging but inconclusive.

It was a lingering objective of this investigation to examine the possible influence of the *global* ULF environment on wave stimulation in the magnetosphere's interior. One part of the motivation for this was the old suggestion by this project's PI that foreshock/shock pulsations, whose region of occupation is time varying with the orientation of the interplanetary magnetic field (IMF), are most likely to reach the magnetopause through specifically subsolar  $Q_{\parallel}$  structure. A second motivation has been the computation, in an earlier study of this project, of the way in which the bow shock is divided into  $Q_{\parallel}$  and  $Q_{\perp}$  sections, showing when the subsolar solar wind flow tube is or is not included in  $Q_{\parallel}$  waves [Greenstadt 1991]. The result is a paper that tries to illustrate comprehensively the likely dependence of ULF generation on the IMF's variable orientation; the bow shock's and magnetosheath's variable involvement; and the seasonal variability of the magnetosphere's orientation to the solar wind. The paper, awaiting print in the AGU anthology of presentations at last year's Chapman conference on ULF phenomenology in Williamsburg, Virginia, is appended to this report.

### *Related Plasma Wave Studies in Foreshock and Magnetosheath*

Foreshock. The foreshock is an integral part of the  $Q_{\parallel}$  shock, at least at typical Mach numbers  $> 3$ . Outside Earth's, curved, global bow shock, however, the foreshock is by no means uniform in its constituents or their intensities, as we have learned from experience with the low-M shock of the far flank seen by ISEE 3. Shocklets and whistler wave packets, for examples, do not seem to be part of the  $Q_{\parallel}$  profile of shock crossings on the far flanks [Greenstadt *et al.*, 1992]. A sensitive monitor of upstream activity is found in plasma wave measurements, either electron pw oscillations or signals in the ion acoustic

range (IAR) of frequencies. Since pw waves are indicative of mixed nonequilibrium plasma components, we have undertaken to examine the pw prevailing spatial signatures of  $f_{pe}$  and IAR signals in the foreshock as diagnostics of return electron and ion populations. We are using a foreshock mapping program developed by Crawford at UCLA for analysis of the Venus pw foreshock with Pioneer Venus Orbiter data. As this is written, the first look at  $f_{pe}$  data is being studied, and we hope to complete a preliminary survey with funds from another project, and have proposed support for additional work IAR data as well. An abstract of a presentation to be given at the December 1993 AGU meeting in San Francisco is attached.

Magnetosheath. A major puzzle that has occupied us for some time is the prevalence of pw IAR-noise far downstream from the bow shock in the magnetosheath, where plasma distributions ought to have reached equilibrium, at least most of the time. In fact the distant downstream noise tends to be just as intense as the noise at the shock itself. In collecting cases from ISEE 3 to illustrate this phenomenon, however, we observed several instances in which pw noise was virtually absent immediately behind the shock crossing. Further examination of the data disclosed that pw dropouts were also common near and far downstream, although high amplitude signals were the rule. These dropouts were found to correlate highly with orientation of the local, ambient field in the sheath across the basically antisolar flow direction of the plasma. That is, the pw signals diminished or disappeared when the angle  $\theta_{XB}$  between the SEC X-axis and  $\mathbf{B}$  approached  $90^\circ$ . At the present time, we have not arrived at an explanation for the pw attenuations, but it seems probable that  $Q_{\parallel}/Q_{\perp}$  variation in the bow shock system is involved and that the dropouts offer the key to understanding the more customary presence of high pw noise levels in the sheath. Continued investigation and a preliminary report will be prepared under sponsorship of another, short-lived program, and a proposal for a more extensive investigation has been submitted. An abstract of a presentation to be given at the December 1993 AGU meeting in San Francisco is attached.

### Recommendations

Thirty years, roughly, of discovery of and research into the nature of collisionless shocks in space, particularly of their  $Q_{\parallel}$  form, which was unknown until recorded by satellite instruments, have advanced our understanding of these phenomena from speculative or unexpected to reasonably knowledgable, if not completely comprehending. The space plasma community has been aided in recent years by increasingly sophisticated numerical simulations of complicated shock profiles. These have succeeded at least in creating approximations to real shocks open to repeated experiments with controlled plasma parameters. Nevertheless, certain long standing issues remain unresolved. Essentially some pages of the shock story have been illuminated without yet becoming quite legible. Although each investigator may have a different perspective on what remains to be done, three subjects still remain at the center of our attention. These are:

Q<sub>||</sub> Development and Structure. Q<sub>||</sub> reformation, involving the interaction of backstreaming ions, solar wind ions, and convected upstream waves, has become highly variable because, a., several groups of simulators have arrived at substantially similar representations of the shock profile using somewhat different models and techniques, and b., the results bear a resemblance to observed signatures of the Earth's bow shock. Unfortunately, numerical experiments have outrun the diminishing efforts of observers to validate simulators' results for two reasons: existing data from past satellite flights have been insufficiently exploited, and past ion sensors have not provided sufficient resolution to characterize shock particle components finely enough either in time sequence or phase space. We recommend strongly that the balance between observation and simulation be restored by increased support for attempts to dissect the details of the hundreds of Q<sub>||</sub> shock crossings in existing high resolution magnetic field, plasma wave, and electron data bases, supplemented by the best ion measurements available,

Ion Acoustic Range Instabilities. Plasma wave activity at intrinsic or doppler-shifted IAR frequencies have been ubiquitous in space measurements not only in shocks but in almost every identifiable space plasma regime. Yet in many cases, not all with the same combinations of parameters, the conditions for classic ion acoustic instability are not satisfied, or as described above for the magnetosheath, the activity persists where it should itself have squelched the disequilibria that are presumed to have generated it. This subject is fundamental and deserves further attention. We therefore recommend support of theoretical efforts to explain IAR pw signals by investigators working closely with the highest resolution observational data currently available.

ULF Waves in Earth's Plasma Environment. There can hardly be two phenomena in space so spatially remote from each other, yet so clearly linked, as ULF waves associated with the bow shock and ULF waves in the magnetosphere. But we still have established neither the mechanism(s) nor even the pathway(s) by which wave energy is transferred from the solar wind-foreshock-shock-magnetosheath system to the magnetosphere, although some routes have been suggested. We believe that pending launches of coordinated satellites, should they be fully successful, will be very helpful in advancing our knowledge of the global wave transfer process, but there are many massive, existing data bases which will *not* be appreciably augmented in the foreseeable future, and whose analysis is highly promising. We recommend support of projects directed at untangling the global properties of ULF wave transfer using accumulated observational records from satellites and surface stations.

#### References

Greenstadt, E. W., Quasi-parallel/quasi-perpendicular divisions of Earth's bow shock, *J. Geophys. Res.*, 96, 1697, 1991.

Greenstadt, E. W., and M. M. Mellott, Variable field-to-normal angles in the shock/foreshock boundary observed by ISEE 1 and 2, *Geophys. Res. Lett.*, 12, 129, 1985.

Scholer, M., and D. Burgess, The role of upstream waves in supercritical, quasi-parallel shock reformation, *J. Geophys. Res.*, *97*, 8319, 1992.

#### Reports and Technical Presentations

##### *Reports.*

Greenstadt, E. W., S. L. Moses, F. V. Coroniti, M. H. Farris, and C. T. Russell, The quasiperpendicular environment of large magnetic pulses in Earth's quasiparallel foreshock: ISEE 1 & 2 observations, *Geophys. Res. Lett.*, *20*, 1459, 1993.

Greenstadt, E. W., and C. T. Russell, Stimulation of exogenic, daytime, geomagnetic pulsations: A global perspective, *AGU Monograph: Solar Wind Sources of Magnetospheric ULF Waves*, in press, Dec., 1993.

Coroniti, F. V., S. L. Moses, E. W. Greenstadt, B. T. Tsurutani, and E. J. Smith, Magnetic and electric field waves in slow shocks of the distant geomagnetic tail: ISEE 3 observations, *J. Geophys. Res.*, *submitted*, 1993.

##### *Presentations.*

Moses, S. L., E. W. Greenstadt, F. V. Coroniti, and B. T. Tsurutani, Plasma waves in distant tail slow shocks, presented at the Fall Meeting of AGU, San Francisco, December, 1992.

Greenstadt, E. W., S. L. Moses, F. V. Coroniti, M. Farris, and C. T. Russell, The quasiperpendicular environment of large amplitude magnetic pulses in Earth's quasiparallel bow shock: ISEE 1 and 2 observations, presented at the Fall Meeting of AGU, San Francisco, December, 1992.

Moses, S. L., F. V. Coroniti, E. W. Greenstadt, Magnetic field direction control of plasma wave emissions in the Earth's magnetosheath, presented at the Fall Meeting of AGU, San Francisco, December, 1993.

Greenstadt, E. W., S. L. Moses, F. V. Coroniti, G. K. Crawford, R. J. Strangeway, Electron plasma oscillations in the foreshock: Comparison of occurrence at PVO and ISEE 3, to be presented at the Fall Meeting of AGU, San Francisco, December, 1993.

THE QUASIPERPENDICULAR ENVIRONMENT OF LARGE MAGNETIC PULSES  
IN EARTH'S QUASIPARALLEL FORESHOCK: ISEE 1 & 2 OBSERVATIONS

E. W. Greenstadt, S. L. Moses, F. V. Coroniti<sup>1</sup>

Electromagnetic Technology Department, TRW Inc.

M. H. Farris and C. T. Russell

Dept. of Earth and Space Sciences, UCLA

*Abstract.* ULF waves in Earth's foreshock cause the instantaneous angle  $\vartheta_{Bn}$  between the upstream magnetic field and the shock normal to deviate from its average value. Close to the quasiparallel ( $Q_{\parallel}$ ) shock the transverse components of the waves become so large that the orientation of the field to the normal becomes quasiperpendicular ( $Q_{\perp}$ ) during applicable phases of each wave cycle. Large upstream pulses of  $B$  were observed completely enclosed in excursions of  $\vartheta_{Bn}$  into the  $Q_{\perp}$  range. A recent numerical simulation included  $\vartheta_{Bn}$  among the parameters examined in  $Q_{\parallel}$  runs, and described a similar coincidence as intrinsic to a stage in development of the reformation process of such shocks. Thus, the natural environment of the  $Q_{\parallel}$  section of Earth's bow shock seems to include an identifiable class of enlarged magnetic pulses for which local  $Q_{\perp}$  geometry is a necessary association.

Introduction

Waves associated with locally quasiparallel ( $Q_{\parallel}$ ) structure in Earth's foreshock and bow shock cause the angle  $\vartheta_{Bn}$  between the upstream field  $\mathbf{B}$  and the nominal shock normal  $\mathbf{n}$  to vary between wide extremes. Greenstadt and Mellott [1985] noted that the defining boundary between solar wind and magnetosheath seemed to be consistently characterized by high, average  $\vartheta_{Bn}$ , i.e., quasiperpendicular ( $Q_{\perp}$ ) geometry, just outside and downstream from the boundary. They also noted that some large amplitude pulses in field strength typical of  $Q_{\parallel}$  phenomenology upstream from the shock seemed to be accompanied, if not actually enclosed, by excursions of  $\vartheta_{Bn}$  into the  $Q_{\perp}$  range ( $45^{\circ} < \vartheta_{Bn} < 90^{\circ}$ ). However, they examined only a few cases and only with 12-s averaged data from the ISEE 1 and 2 magnetometers in 4-s/average plots. In some cases the rises in  $B$  ( $\equiv |\mathbf{B}|$ ) and  $\vartheta_{Bn}$  were virtually simultaneous, so details were lost in the early survey.

Since the earlier report, some simulators have included local, or instantaneous,  $\vartheta_{Bn}$  among the variable parameters they examined [Thomas et al., 1990; Winske et al., 1990]. Most notably, a recent one-dimensional simulation found a definite connection between enlarged  $\vartheta_{Bn}$  and

the point in the history of a convecting upstream wave where it encounters reflected beams [Scholer and Burgess, 1992]. This report demonstrates that a locally  $Q_{\perp}$  environment surrounded a set of independently selected upstream pulses when these are examined at the highest resolution available to the ISEE 1 and 2 instruments. Our results are compatible with recent simulations and a scenario for pulse development at the  $Q_{\parallel}$  bow shock.

Data

The examples of this report are represented by magnetic field measurements sampled 4 or 16 times per second, depending on the rate in effect at the time of observation, using the UCLA fluxgate magnetometers of ISEE 1 and 2 [Russell, 1978]. Shock normals have been calculated from both the model of Greenstadt et al. [1990] at the positions of shock crossing and coplanarity results obtainable from the locally varying, hence not very reliably represented, downstream components. For pulses and the upstream fields in which they occurred, the normals were calculated for the spacecraft locations at the times of nearest corresponding shock crossings, but directions of the solar wind's IMF were averaged for intervals just upstream from significant foreshock activity in an attempt to evade changes in the measured field components influenced by the foreshock itself, particularly its pulses. No  $\vartheta_{Bn}$  should be taken as an exact value, but only as confirmation that the corresponding shock/foreshock system was as  $Q_{\parallel}$  at the closest time of undisturbed IMF as its deeper signature indicated.

Most of the examples are represented as paired time plots of field magnitude and normal angle. Samples from both ISEE 1 and 2 are shown, some for the same data intervals, in which somewhat dissimilar records from the separated spacecraft offer semi-independent results.

Examples

*Shock context and crossings*

Figure 1 displays a compressed plot of foreshock phenomena "typical" of a long enough ( $> 15$  min.) approach to a  $Q_{\parallel}$  shock to suggest relatively steady upstream conditions. Outside the figure to the left,  $\vartheta_{Bn} \approx 19^{\circ}$  upstream from major excursions of  $\mathbf{B}$  in the foreshock. We see increases in field magnitude, wave frequency, wave amplitude, pulse amplitude, and pulse incidence as ISEE 1 nears the magnetosheath at the right of the figure. By "pulses" throughout this report we mean temporary rises in  $B$  to levels comparable to downstream

<sup>1</sup>Permanent address: Dept. of Astronomy, UCLA, Los Angeles, CA 90024.

## **Unpublished Reports**

# Stimulation of Exogenic, Daytime Geomagnetic Pulsations: A Global Perspective

E. W. GREENSTADT

*Electromagnetic Technology Dept., TRW, Redondo Beach,  
California*

C. T. RUSSELL

*Dept. of Geophysics and Planetary Physics, Univ. of  
Calif., Los Angeles*

The long history of observations and concepts in the process of trying to understand the linkage between solar wind parameters and daytime ULF pulsations in the range of  $f$  between, roughly, 7 and 70 mHz, has produced statistical studies persuasive of that linkage, but with weak correlations and imprecise, even unspecific, conclusions regarding the locales and mechanisms of physical connection between perturbations outside the magnetopause and oscillations inside the magnetosphere. We believe part of the difficulty lies in the asymmetries and temporal variabilities that affect, individually and together, the foreshock, bow shock, magnetosheath, magnetopause, and magnetosphere through which the progress of ULF stimulation and maintenance must pass. We summarize the asymmetric distributions of hypothesized sources and magnetospheric sites of ULF excitation and the continual, diurnal, and seasonal variation that must affect such excitation, including the asymmetries of foreshock, bow shock, and sheath, and the time-dependent orientation of the magnetosphere to the solar wind. We suggest that the nonuniform and nonstationary factors described, although adding complexity to the overall solar-geomagnetic system, should be taken into account by future investigations with appropriately selected subsets of data. Then the relationship between at least some magnetospheric ULF phenomena and their external sources will be clarified.

## INTRODUCTION

Oscillations of a few tens of seconds period and striking quasinusoidal regularity are commonly, but not continuously, detected on Earth's surface and in the magnetosphere, magnetosheath, and solar wind outside Earth's bow shock by magnetometers sensitive to changes of ambient magnetic flux greater than one nanotesla. Consequently, ULF waves occurring in the geomagnetic environment are subjects of observation, theory, and speculation as old as the instruments capable of recording them. Magnetospheric waves that occur in local daylight hours have been linked many times to various combinations of solar wind parameters. Although the solar wind can exert control on the occurrence and properties of ULF pulsations in many ways, however, the history of the subject has usually given us widely scattered points in observational correlations and conflicting conclusions in theoretical studies, so that many questions remain. Are all spectrally comparable oscillations unrelated to one another but coincidentally similar? Or are they related to each other by a common generator, and if so, how? Or are they in fact all displays of the same phenomenon travelling through different locations with slightly different local characteristics?

Despite the many uncertainties, some classes of magnetospheric waves have been fairly well explained; the reader will not be tranquilized with these here. The subject of this essay is day time geomagnetic pulsations in what has traditionally been designated the Pc3/Pc4 period ranges 15-45/45-150s, where no one today doubts that an external source of Pc3-4's operates, but where uncertainty and conflict still prevail. A little bit of history

angle  $\theta_{XB}$  in determining the pattern of ULF occurrence around the curved bow shock, where  $\theta_{XB}$  is the "cone angle" between the field vector and the solar wind flow. The flow direction is approximated by the solar ecliptic  $\pm X$  direction independent of sense.

The cone angle concept is that wave phenomenology attendant on the ULF component of quasiparallel shock structure increasingly dominates the subsolar region of the bow shock as  $\theta_{XB}$  drops below about  $51^\circ$ . Oscillating and turbulent, or quasiparallel ( $Q_{\parallel}$ ), structure characterizes the bow shock where the angle  $\theta_{Bn}$  between the IMF  $\mathbf{B}$  and the local shock normal  $\mathbf{n}$  is less than  $\sim 51^\circ$ ; a steplike, quasiperpendicular ( $Q_{\perp}$ ), structure relatively free of ULF signals characterizes the shock where  $\theta_{Bn} > \sim 51^\circ$ . Subsolar  $Q_{\parallel}$  structure fills with oscillations the central solar wind flux tube whose plasma later grazes the magnetopause, transferring its waves to the magnetosphere.

The model assumes rotational symmetry, around the X-axis, of the shock and wave-pulsation relationship. Thus the cone angle combines the latitude and longitude of the IMF vector favored by the early Russian work, since  $\cos \theta_{XB} = \cos(\text{lat}B) \times \cos(\text{long}B)$ . Sketches illustrating this postulate accompany a later section of this report. The point here is that scatter diagrams developed by different investigators with different data bases, attempting to quantify pulsation activity by amplitude as well as occurrence, supported this model, but with rather poor statistical correlation. This can be readily appreciated, even for the best relationships of occurrence or amplitudes vs.  $V_{SW}$ , in Figure 2.

Compressional wave energy in the magnetosheath, derived from wave-particle interactions in the foreshock and shock, can presumably be transferred to the magnetosphere simply by periodic pressure variation at the magnetopause. Such stimulation could also arise from wavetrains delivered from the solar wind itself, but periodic oscillations are not the only available pressure phenomena. Nonperiodic pressure variations, including pulses and discontinuities, are intrinsic to the solar wind; also, long term ( $T > 1000s$ ) variations of the IMF cause unsteadiness and relocation of the foreshock. Either may impinge on the magnetopause. There can also be inherent unsteadiness in the interaction between the shocked solar wind and the magnetopause.

All aspects of ULF wave stimulation are subject to prevailing conditions in the global magnetospheric environment. We describe this environment before discussing the specific sources of wave generation and transfer in which they must operate.

#### THE GLOBAL WAVE-TRANSFER ENVIRONMENT

The lingering uncertainty surrounding generation of daytime ULF activity stems from the inherent complexity of space plasmas and the recognized proliferation of subregions in the Earth's interaction with the solar wind. The subregions in this overview, within their dynamic environment, are the rotating magnetosphere, enclosed by the magnetopause, within the solar wind flowing by in the magnetosheath, modified by having passed through the bow shock/foreshock system, whose wave profiles are controlled by the continuously varying interplanetary magnetic field. We shall work outward from the magnetopause.

### *Magnetopause*

The magnetopause is nonuniform. It is approximately bilaterally (geomagnetically East-West) symmetric with respect to the X-Z plane of the solar wind flow (X) and the magnetic pole ( $Z_M$ ), but does not in general present a symmetric boundary to the magnetosheath flow within or parallel to that plane. There are even dissimilar boundary zones in the conventional symmetric configuration, as follows:

*The symmetric case.* Figure 3E, upper right (E for equinoctial), is a simplified, conceptual X-Z cross section of the magnetosphere when it is in a nominally static, symmetric, magnetically untilted orientation behind the bow shock. Notation "1, 2, 3" calls attention to three distinct regions of the boundary that may have distinct responses to the imposition of perturbed magnetosheath plasma on the magnetopause. The three boundary areas are:

1. *Equatorial (Axial Stagnation).* In this region, the flow of the solar wind close to the subsolar point where the axis of symmetry intersects the magnetopause is presumably at or near zero velocity. Waves present here, particularly pressure waves, or pulses, may stimulate the magnetopause at their prevailing frequencies and propagate directly into the equatorial magnetosphere as compressional waves crossing the earth's field lines.

2. *Midlatitude (Anaxial Streamflow).* Away from the stagnation region, the solar wind has nonzero speed parallel to the magnetopause. Waves crossing at any point may impart to their magnetospheric successors a tangential  $k$ -vector component influenced by their convection velocity along the boundary. Propagation might be primarily along outer field lines toward higher latitudes (or, in an equatorial X-Y cross section, toward dawn and dusk terminators).

3. *Cusp (Penetration).* In the cusp region, tangentially flowing, hot solar wind plasma may penetrate the magnetopause directly, carrying any periodic modulations within it deep into the magnetosphere at auroral and cusp latitudes.

Each of the above combinations of local magnetopause configuration and magnetosheath activity acts on its own local version of the magnetopause boundary layer or mantle; each version has its own effects, if any, on the transmission of waves. Additional regions and modes of transfer can be postulated, and, of course, counterparts of these around an equatorial cross section may also be suggested. Not all parts of the magnetosphere's boundary can be expected to receive the same stimulation, or have equal sensitivity to whatever outside perturbations come to them, even within this depiction of what has been the traditional zero-order conception of a static and symmetric magnetosphere.

*The asymmetric case.* In general the magnetosphere is neither static nor symmetric with respect to the Sun-Earth line. More representative, asymmetric diagrams are becoming common [Walker et al, 1989; Kivelson and Hughes, 1990], and recognition of the magnetopause's time-variable orientations to its external wave environment may be as important as recognition of its subregions. Just as we expect substorm processes and reconnection to depend on the instantaneous orientation of the magnetosphere to the solar wind, we should not be surprised if geomagnetic pulsations too depend on orientation of the subregions to the magnetosheath flow.

The diagram at the left center of Figure 3 is a schematic projection of the magnetic pole's trajectory on the ecliptic plane through an annual cycle, combining both its seasonal and diurnal dynamics. In this diagram, borrowed from Kivelson and Hughes [1990], the effect of annual and daily tilt on the orientation of the magnetosphere to the solar wind is explicit for some sample times a quarter-year and six hours from one another, and can be inferred for any other times. If we imagine ourselves looking down from the North ecliptic pole with the sun at left of the page, we see that the North magnetic pole can tilt from  $34^\circ$  ( $23^\circ + 11^\circ$ ) toward the sun at northern summer solstice in June (left point SS, at 1640) to  $34^\circ$  away from the sun at northern winter solstice in December (right point WS, at 0440). Such differing orientations expose the cusp, say, to different regions of the interaction boundary at different times. Thus, entirely different sections of the magnetopause may be affected at one time compared to another, even for identical distributions of magnetosheath disturbance. This is the argument illustrated explicitly in the two large diagrams of the figure, that is, in the pair of meridian cross sections E and SS. Magnetosphere E corresponds to the equinox times E, and magnetospheric sketch SS to noontime of summer solstice of the left-center diagram.

In Figure 3SS, region 2 of the tilted magnetosphere, not region 1 as in 4E, faces the stagnation point of the magnetosheath and region 3 is also reoriented to confront a less deflected, perhaps more penetrating, solar wind than it does in E. Below the axis of symmetry, notations 2' and 3' have been substituted for 2 and 3 to emphasize the asymmetry in SS of corresponding north and south magnetic latitudes with respect to the solar wind, unlike their symmetric counterparts in Figure 3E. We can easily imagine a mirror image of Figure 3SS, rotated  $180^\circ$  around the X-axis, showing the approximate magnetospheric orientation at the opposite, winter solstice, (WS), with the south geographic and magnetic poles tilted sharply toward the sun.

Clearly the seasonally corrected magnetosphere presents the different areas (1,2,3) of its envelope to the subsolar flow and its convected magnetic oscillations in quite different postures, and we may reasonably expect waves in the magnetosphere to show different patterns of response, most clearly distinguishable during the seasonal extremes and perhaps more subtly during intermediate times. Seasonal variation of Pc3 activity in the central magnetosphere was derived statistically from data recorded by the geosynchronous satellite ATS 6 [Takahashi et al., 1981], and data bases from such sources may still prove valuable if revisited in the context of Figure 3.

The shaded streamlines through the subsolar area of the shock in Figures 3E & SS, adapted from calculations by Spreiter and Alksne [1969], illustrate a sample projected boundary of a column, or cylinder, of solar wind that flows through the subsolar region and spreads in the magnetosheath to flow within  $1 R_E$  of the flank magnetopause at the terminators,  $90^\circ$  from subsolar point. We may imagine the actual activity in the magnetosphere to depend on combinations of periodic diurnal and seasonal circumstances, such as those of Figure 3 and on the sources of disturbance in the magnetosheath: that is, on the transient global distributions of activity in the layer of plasma flowing over the magnetosphere's surface.

### *Magnetosheath*

The source of those waves in the magnetosphere that derive from external stimulation lies in the magnetosheath. At any given time the magnetosheath contains a nonuniform, global distribution of perturbations whose relationship to the magnetopause determines where and how much, if any, of their energy will be transferred into the magnetosphere. What are the prevailing distributions of disturbance around the magnetopause when the waves are in progress--and when they are not?

We know the answer to this question for certain extreme and specialized situations, namely when the magnetopause is likely to be engulfed in waves convected from upstream, and when it is likely to be surrounded by no convected waves at all [Greenstadt, 1973; Russell et al., 1983]. In the former case, daytime waves are abundant; in the latter, they are absent [Wolfe, 1980; Wolfe et al., 1980]. Figure 4 depicts these two extremes, exhibiting incidentally the contrasting specialized orientations of the interplanetary magnetic field (IMF) that support them. The sketches are derived from the MHD calculations of Spreiter and Alksne. [1969].

In 4a, at left, the IMF and the SW flow are parallel (IMF cone angle  $\theta_{XB} = 0^\circ$ ); the field and plasma follow identical flow lines in the magnetosheath, with the lines deflected around the magnetopause. Only lines near the axis of symmetry, i.e., near the X-axis, come close to the magnetopause, as illustrated in the previous figure.

In 4b, at right, the IMF is oriented perpendicular to its orientation in 4a ( $\theta_{XB} = 90^\circ$ ), while the SW flow, not depicted explicitly, is the same as in 4a. Here, the field lines are draped around the magnetopause, and all of them come near the subsolar magnetopause in their turn, slipping around the magnetopause above or below the plane of the sketch or merging with magnetospheric field lines as the sense of the magnetic vectors might dictate (northward as in the panel, or at times southward). The field lines are drawn as wavy to illustrate the paths along which foreshock and shock perturbations should be expected to reach the daylight magnetopause easily in 4(a) but with difficulty in 4b. The dashed lines in 4b represent the boundaries of the ULF foreshocks for the  $90^\circ$  IMF orientation.

Cases 4a and b are strongly associated with presence or absence of daytime magnetospheric pulsations, respectively. These extremes are infrequent, however, and statically idealized. On ordinary days the more general magnetosphere is moderately excited, and its waves may be related to the time-varying distributions in the sheath of each parameter of each component of the sheath plasma, such as density of the ions, temperature of the electrons, or strength of the magnetic field, and of the pattern of spectral power of the variations of each of these parameters everywhere in proximity to the magnetopause. Meanwhile, there are additional complications that affect the magnetosheath.

### *Bow Shock and Cone Angle*

Recent study of the divisions between  $Q_{\perp}$  and  $Q_{\parallel}$  structures on the bow shock make it possible to replace or supplement the generic shock-origin sketches of Figure 4, [Greenstadt 1973; Russell et al. 1983; and the widely circulated cover of the Upstream Waves and Particles issue of *J. Geophys. Res.* 86, June 1, 1981] with more refined configurations. One such configuration, for the most probable  $45^\circ$  cone angle of the IMF,

will be described here, along with a pair of deviations. More complete sketches of the  $Q_{\perp}/Q_{\parallel}$  divisions for a selection of cone angles have been published elsewhere [Greenstadt, 1991]; extrapolation of the reasoning below to such configurations can be easily constructed, while the extremes sketched in Figure 4, which correspond, to  $\theta_{XB} = 0^{\circ}$  and  $90^{\circ}$  remain essentially unaffected.

The most probable or "typical" state of the bow shock is illustrated in Figures 5a and b. The IMF is assumed to be in the ecliptic plane at the Parker spiral angle,  $\theta_{XB} = 45^{\circ}$ , and the transition between  $Q_{\perp}$  and  $Q_{\parallel}$  structures is assumed to occur wherever on the shock the local  $\theta_{Bn} = 51^{\circ}$  [Diodato et al., 1976; Greenstadt, 1991]. Panels a and b of the figure show the projections on the X-Y and Y-Z planes, respectively, of the boundaries between  $Q_{\perp}$  and  $Q_{\parallel}$  sections of the shock, with the fully  $Q_{\parallel}$  section darkly shaded and the section timeshared between  $Q_{\parallel}$  and  $Q_{\perp}$  signified by darker shading. The timeshared section is meant to represent the area where waves at the shock modify  $\theta_{Bn}$  locally so that the shock is  $Q_{\perp}$  during some part of each wave period and  $Q_{\parallel}$  during the other part.

We see that a portion of the morning side of the shock is  $Q_{\parallel}$ , and that there is a small intrusion of the timeshared structure into the afternoon shock around the subsolar point. The circle around the origin in b represents the boundary of the cylinder whose flow passes within  $7 R_E$  of the subsolar point and then, according to the drawings of Spreiter and Alksne [1969], approximately  $1 R_E$  from the magnetopause terminator. We see that a portion of the plasma in the central flow tube is  $Q_{\parallel}$ , another portion borderline  $Q_{\perp}/Q_{\parallel}$ , and yet another entirely  $Q_{\perp}$ . Some  $Q_{\parallel}$  activity is carried to within  $1 R_E$  of the dawn terminator and some borderline wave activity bathes the entire magnetopause, but no continuous  $Q_{\parallel}$  wave activity is convected to the dusk terminator.

Figures 5c and d represent the Y-Z projections for less probable, but by no means rare, stream angles  $30^{\circ}$  and  $60^{\circ}$ . The sketch in 5c encourages the idea that most of the subsolar flow column, perhaps all of it, if we were to include the comparable  $Q_{\perp}/Q_{\parallel}$  timeshared region, as in 5a, would be occupied by ULF wave signals in contact with most, if not all, of the daytime magnetopause when the stream angle is  $30^{\circ}$ . The sketch of 5d, in contrast, supports the expectation that even with an additional  $Q_{\perp}/Q_{\parallel}$  region, only a section of the subsolar flow column and a corresponding section of the morning magnetopause would be in contact with outside ULF activity when the stream angle is  $60^{\circ}$ . These two cases represent the limits, more or less, of stream angles below or above which geomagnetic pulsations might be stimulated all day or at no daylight hours by solar wind-convected ULF activity.

Two more complications merit attention in this synopsis of the ULF environment. First, the wavy horizontal lines in the upper panel of Figure 6 define another subsection of the shock where the shock is presumably  $Q_{\perp}$  because  $\theta_{Bn} > 51^{\circ}$ , but where observations have shown foreshock waves generated by reflected ions are convected back to the shock for the  $45^{\circ}$  orientation of the IMF [Greenstadt, 1991]. The Y-Z projection of this region is indicated by the wavy lines in the lower panel. Second, the three irregular and nonuniform grades of shading in both sketches is intended to portray the nonuniformity of the  $Q_{\parallel}$  structure, with darker shade meaning more parallel geometry

and larger amplitude, more compressional oscillations than the lighter shades. In the lower panel, the larger circle marked M and the smaller circle marked F indicate the nominal sizes of the Y-Z cross section of the magnetopause and the subsolar flow tube passing within  $1 R_E$  of M in the upper panel. The nonuniform shading emphasizes superposition of these qualitative complications on the computed  $Q_{\perp}/Q_{\parallel}$  boundary and on magnetosheath flow lines downstream. Thus the global distribution of shock- or foreshock-related disturbance in the subsolar flow tube of the magnetosheath and consequently around the magnetopause is unmistakably asymmetric.

We must imagine that some waves of small to moderate amplitudes in the leading edge of the  $Q_{\parallel}$  region might reach the magnetopause largely in the morning sector above and below the ecliptic plane, for the illustrated configuration. Their power would be averaged over the expanded cross section of the tube at the magnetopause, so we would not expect an overwhelming response inside the magnetosphere. Decreasing cone angles would place an increasing supply of larger amplitude waves inside the tube on both evening and morning sides, and at high (polar) as well as low (ecliptic) latitudes. Increasing cone angles would remove significant waves from the subsolar tube and therefore from the vicinity of the magnetopause. The response of the magnetosphere would then be presumed to depend on which regions of the magnetopause would be exposed to the perturbations in the flow, as implied in Figure 3. Some regions might be as sensitive to small disturbance when, say,  $\theta_{XB} = 50^{\circ}$  as others to larger disturbance when  $\theta_{XB} = 30^{\circ}$ .

#### *Temporal change*

Before proceeding to the actual machinery of wave energy-transfer, we emphasize that all the global configurations and processes are in continuous variation caused, in simplest terms, by the rotations of the Sun and Earth, so that the former presents a dynamic plasma source of the rapidly changing solar wind, while the latter offers a diurnal and seasonally changing asymmetry to the portion of solar wind conveyed to it. Thus the actual situation is a time-dependent selection from an infinite number of configurations such as the static cases sketched in the Figures.

#### *Wave transfer*

The large and intricate subject of the actual mechanisms by which ULF energy might be physically transferred from the solar wind to the magnetosphere cannot be detailed here, but some of the evidence supporting the main hypotheses can be outlined. Broadly speaking, there are two instigators of magnetospheric oscillation: more or less continuous wavetrains and pressure impulses or irregular transients impinging on the magnetopause. Wavetrains may occur as any combination of transverse and compressional, narrow or broadband, oscillations.

The conceptually simplest hypotheses of wave transfer apply to wave trains. The transverse components of a monochromatic wave vector can be imagined, given the appropriate orientation of  $\mathbf{k}$ , to alternately reinforce and oppose the geomagnetic field lines at the magnetopause, creating small scale, local signals, or even disconnections and reconnections or mini-flux transfer events [FTEs, Russell and Elphic, 1978; see next subsection, below]. These signals might then propagate along the

lines and/or deep into the magnetosphere where, upon encountering lines of the same natural frequency, they would initiate or drive a geomagnetic resonance oscillation. Alternatively, or supplementally, the compressional part of a magnetosheath wavetrain might initiate a pressure signal that would penetrate the magnetosphere with the same result.

The weaknesses of this simple concept lie in satellite observations, which have not revealed monochromatic wavetrains in the deep magnetosheath that would correspond to the common occurrence of such waves inside the magnetosphere, and, moreover, have revealed harmonic structures of pulsations inside the magnetosphere that suggest a multichromatic source. The more probable form of external wave stimulation is by the typically broadband signals in the sheath, from which the magnetosphere allows internal propagation and selects resonances when the appropriate field lines or shells are crossed by the penetrating signal.

Nothing in the above concepts enlightens us regarding the actual site(s) of transfer of external to internal wave energy, which could be anywhere from subsolar to flank or polar locations. We do know, both theoretically [Verzariu, 1973; Wolfe and Kaufmann, 1975] and observationally [Greenstadt et al., 1983; Tomomura et al., 1983] that wave power just inside the dayside magnetopause can be orders of magnitude less than the power just outside in the sheath, at least for certain well defined magnetopause models or a few chance locations of measurement. Other models, locations, or roundabout transfer routes are not ruled out, however. Recent reports of investigations by Engebretson et al. [1991] and Lin et al. [1991] have included summaries of such proposed mechanisms.

One model would have compressional oscillations in the foreshock propagate directly through the shock, sheath, and subsolar magnetopause into the lower magnetosphere [Yumoto and Saito, 1983; Yumoto et al., 1984; Russell et al., 1983]. Another suggests that waves enter along cusp/cleft/boundary layer field lines [Troitskaya and Bol'shokova, 1984] and then transfer to the interior dayside magnetosphere via an ionospheric process [Lanzerotti et al., 1972; Engebretson et al., 1990]. Either or both are supported to some degree by satellite evidence. Figure 7 presents some of the support for these suggestions. All plots in the figure show scatter diagrams consistent with the well known and long standing relationship between the strength of the IMF and the period of daytime geomagnetic pulsations [Gul'elmi et al., 1973; Vero and Hollo, 1978]. Compatible versions of the relationship are offered in the three upper panels [Yumoto et al., 1984] at geosynchronous (GOES) and two low-L surface stations, and in the bottom panel [Engebretson et al., 1986] at a polar station south of the auroral oval. The  $f-B_{SW}$  dependence results from particle-wave interactions at local cyclotron frequencies in the solar wind around the bow shock. It's difficult to explain such uniform action within the magnetosphere, where local resonance frequencies should have differed from one another significantly, without invoking direct transfer of some of the original signal to all sites. Of course, the data don't tell us whether the pathway was around the cusp and inward to the equator and the pole via the ionosphere or through the subsolar magnetosphere and outward to the cusp field and beyond.

If either model applies, the seasonal presentation of the equator or cusps to the patterns of disturbance in the sheath must

surely play a role in the efficiency of these pathways and the parts of the magnetosphere most readily affected. Seasonality would contribute scatter to the relationships.

#### *Pressure variation*

Changes in the solar wind and its embedded IMF could be responsible for pulsations inside the magnetosphere stimulated by irregular, rather than periodic, pressure variations at the magnetopause. Statistical evidence for a dual dependence of Pc3-4 period on solar wind density  $N_{SW}$ , decreasing with  $N_{SW}$  for Pc3, increasing for Pc4, was developed, for example, by Gringauz et al. [1970]. Since we treat here mainly with sustained, rather than transient pulsations, we skip lightly over impulses, such as interplanetary shocks, as sources. Daytime pulsations in the frequency range we describe have not been shown to correlate strongly with solar wind pressure pulses or discontinuities. Oscillations induced by impulses are essentially transient or damped [Saito and Matsushita, 1967] and, moreover, when sustained, may result from other changes in IMF geometry that happen to accompany the impulse. There are, however, inherent pressure changes at the magnetopause and driven pressure changes from the shock system that, though irregular, are not isolated and might be responsible for sustained effects in the magnetosphere.

Pressure variation associated with unsteadiness of the magnetopause could be due to a fluid instability such as the Kelvin-Helmholtz (K-H) instability or due to a magnetic effect such as time varying reconnection. Since motion of the magnetopause appears to be controlled by the fluctuations in the momentum flux of the solar wind and the southward IMF, as discussed by Song et al. [1988] and illustrated in Figure 8 (their Figure 2), and K-H phenomenology seems to be associated principally with Pc 5 oscillations more at dawn and dusk than midday, we shall not pursue the K-H source here. We consider instead time-varying, "patchy" reconnection in terms of flux transfer events, as sketched in Figure 9. While this model is certainly idealized, it shows that time varying reconnections can lead to 3-dimensional structures that in turn apply time-varying pressure to the magnetopause. This time-varying pressure in turn can lead to magnetospheric oscillations that decay in amplitude away from the magnetopause. The few studies that have been done show that waves are generated from Pc 3 to Pc 5 frequencies, that compressional fluctuations penetrate the magnetosphere further than transverse fluctuations, and that low frequencies penetrate further than high frequencies [Wolfe et al., 1989].

Since the properties of the magnetosheath plasma which abut the magnetopause are expected to control FTE generation, and since the magnetosheath plasma in turn is controlled by the shock and solar wind, we expect that FTE properties are controlled by the solar wind, but we have little information on this other than that the FTE occurrence rate is controlled by the north-south component of the IMF [Berchem and Russell, 1984]. One mode of disguising the FTE effect that we can rule out is that of triggering by fluctuations in the IMF direction. As Figure 10 shows, the IMF can be very steady when an FTE arises. As far as we can tell FTEs arise spontaneously at the magnetopause when the IMF is southward.

Finally, we speculate on an additional pressure effect at the magnetopause, so far unresearched. The solar wind pressure is

reduced inside the compressional wave foreshock all the way to the bow shock. An example of lowered pressure in the foreshock is shown in Figure 11 [Le, 1991]. If this effect is transmitted through the shock and sheath to the magnetopause, it could initiate pulsations in the magnetosphere. Recall that the foreshock continually moves around in front of the curved shock in response to changes in orientation of the IMF brought by the solar wind. Transmission of the solar wind/foreshock pressure boundary to the magnetopause should therefore occur according to the patterns of the foreshock's footprint on the shock, as illustrated in the examples of Figures 5 and 6. The magnetopause would then be subject to a pressure differential continually moving, sometimes gradually, sometimes suddenly, across it, possibly generating oscillatory responses inside the magnetosphere.

Pressure effects, with the possible exception of FTE activity, like the wave effects summarized earlier, should all be influenced by the transient, global configuration of the Earth's magnetoplasma environment.

#### DISCUSSION

The central thesis of this report is that the nonuniformity of the shock and foreshock, including the section of the latter outside the locally  $Q_{\perp}$  geometry, is manifested in the magnetosheath and ultimately in the magnetosphere in ways that can be understood only by combining the shock's nonuniformities with the stream flow in the sheath and the nonuniform sensitivities of the magnetopause, taking into account the time variability of all these elements. With this view in mind, steps can be easily enumerated that might advance the investigation of daytime pulsations using the large, compatible satellite and surface data bases currently available.

Inside the magnetosphere, wave statistics need to be divided into subsets according to common combinations of diurnal, seasonal, locational (i.e. by geomagnetic latitude and L-value), and concurrent solar wind parameters. Progressions of event onsets or correlation coefficients might also be instructive organizers of pulsation data.

Outside the magnetosphere, solar wind observations need to be divided into subsets according to common combinations of IMF cone angle and solar wind plasma parameters. The distribution of foreshock and bow shock generated waves and pressure differentials in the magnetosheath, especially in the part of the subsolar flow tube near the magnetopause, must be computed for these subsets and corroborated where possible by observations in the sheath. Promising pairs of satellite observations in two regions at a time, but without benefit of computed distributions, have been described by Engebretson et al. [1991] and Lin et al. [1991b]; also earlier references therein. Recently, Lin et al. [1991a], referring to transfer across the magnetopause, concluded that "from five events...it seems that the transfer rate differs from one event to another."

Finally, the two classes of subsets, IMF direction and plasma flow, must be compared systematically. It seems promising at this time that by taking into account as many of the seeming complications of shock, sheath, and magnetospheric nonuniformity as possible, the task of explaining the global roots and routes of stimulation of geomagnetic pulsations may be appreciably simplified and hastened.

*Acknowledgement.* Preparation of this review was supported at TRW by NASA contracts NASW-4414 and -4749, and at UCLA by the National Science Foundation under grant ATM 91-11913.

- Berchem, J., and C. T. Russell, Flux transfer events on the magnetopause: Spatial distribution and controlling factors, *J. Geophys. Res.*, **89**, 6689, 1984.
- Bol'shakova, O. V., and V. A. Troitskaya, Relation of the interplanetary magnetic field direction to the system of stable oscillations, *Dokl. Akad. Nauk SSSR*, **180**, 4, 1968.
- Cowley, S. W. H., The causes of convection in the Earth's magnetosphere: A review of developments during the IMS, *Rev. Geophys. Space Phys.*, **20**, 531, 1982.
- Diodato, L., E. W. Greenstadt, G. Moreno, and V. Formisano, A statistical study of the upstream wave boundary outside the earth's bow shock, *J. Geophys. Res.*, **81**, 199, 1976.
- Engebretson, M. J., C-L Meng, R. L. Arnoldy, and L. J. Cahill, Jr., Pc 3 pulsations observed near the South polar cusp, *J. Geophys. Res.*, **91**, 8909, 1986.
- Engebretson, M. J., L. J. Cahill, Jr., R. L. Arnoldy, B. J. Anderson, T. J. Rosenberg, D. L. Carpenter, U. S. Inan, and R. H. Eather, The role of the ionosphere in coupling upstream ULF wave power into the dayside magnetosphere, *J. Geophys. Res.*, **96**, 1527, 1991a.
- Engebretson, M. J., N. Lin, W. Baumjohann, H. Luehr, B. J. Anderson, L. J. Zanetti, T. A. Potemra, R. L. McPherron, and M. G. Kivelson, A comparison of ULF fluctuations in the solar wind, magnetosheath, and dayside magnetosphere 1. magnetosheath morphology, *J. Geophys. Res.*, **96**, 3441, 1991b.
- Fairfield, D. H., and N. F. Ness, Magnetic field fluctuations in the Earth's magnetosheath, *J. Geophys. Res.*, **75**, 6050, 1970.
- Greenstadt, E. W., Field-determined oscillations in the magnetosheath as possible source of medium-period, daytime micropulsations, in *Proceedings of Conference on Solar Terrestrial Relations, April 1972*, 515, University of Calgary, 1973.
- Greenstadt, E. W., Quasi-perpendicular/quasi-parallel divisions of Earth's bow shock, *J. Geophys. Res.*, **96**, 1697, 1991.
- Greenstadt, E. W., and J. V. Olson, A contribution to ULF activity in the Pc 3-4 range correlated with IMF radial orientation, *J. Geophys. Res.*, **82**, 4991, 1977.
- Greenstadt, E. W., H. J. Singer, C. T. Russell, and J. V. Olson, IMF orientation, solar wind velocity, and Pc 3-4 signals: A joint distribution, *J. Geophys. Res.*, **84**, 527, 1979.
- Greenstadt, E.W., I.M. Green, D.S. Colburn, J. H. Binsack, and E.F. Lyon, Dual satellite observations of Earth's bow shock: II. Field aligned upstream waves, *Cosmic Electrodyn.*, **1**, 279, 1970a.
- Greenstadt, E.W., I.M. Green, D.S. Colburn, J. H. Binsack, and E.F. Lyon, Dual satellite observations of Earth's bow shock: III. Field determined shock structure, *Cosmic Electrodyn.*, **1**, 316, 1970b.
- Greenstadt, E. W., M. M. Mellott, R. L. McPherron, C. T. Russell, H. J. Singer, and D. J. Knecht, Transfer of pulsation-related wave activity across the magnetopause: Observations of corresponding spectra by ISEE-1 and ISEE-2, *Geophys. Res. Lett.*, **10**, 659, 1983.
- Gringauz, K. I., V. A. Troitskaya, E. K. Solomatina, and R. V. Shchepetov, The relationship of solar wind variables to periods of continuous micropulsations of electromagnetic field of the earth, *Dokl. Akad. Nauk USSR*, **5**, 1061, 1970.
- Gul'elmi, A. V., T. A. Plyasova-Bakunina, and R. V. Shchepetov, Relation between the period of geomagnetic pulsations Pc 3,4 and the parameters of the interplanetary medium at the earth's orbit, *Geomagn. Aeron.*, **13**, 331, 1973.
- Kivelson, M. G., and W. J. Hughes, On the threshold for triggering substorms, *Planet. Space Sci.*, **38**, 211, 1990.
- Kovner, M. S., V. V. Lebedev, Y. A. Plyasova-Bakunina, and V. A. Troitskaya, On the generation of low frequency waves in the solar wind in the front of the bow shock, *Planet. Space Sci.*, **24**, 261, 1976.
- Lanzerotti, L. J., H. P. Lie, N. A. Tartaglia, Ionospheric Effects on the transmission of ultralow-frequency plasma waves, *Science*, **178**, 499, 1972.
- Le, G., Generation of upstream ULF waves in the Earth's foreshock, *Dissertation*, Inst. of Geophys. and Planet. Phys., University of

- California, Los Angeles, 1991.
- Lin, N., M. J. Engebretson, W. Baumjohann, and H. Luehr, Propagation of perturbation energy fluxes in the subsolar magnetosheath: AMPTE IRM observations, *Geophys. Res. Lett.*, 18, 1667, 1991a.
- Lin, N., M. J. Engebretson, R. L. McPherron, M. G. Kivelson, W. Baumjohann, H. Luehr, T. A. Potemra, B. J. Anderson, and L. J. Zanetti, A comparison of ULF fluctuations in the solar wind, magnetosheath, and dayside magnetosphere 2. field and plasma conditions in the magnetosheath, *J. Geophys. Res.*, 96, 3455, 1991b.
- Plyasova-Bakunina, T. A., Effect of the interplanetary magnetic field on the characteristics of Pc 3-4 pulsations, *Geomag. and Aeron.*, 12, 675, 1972.
- Russell, C. T., and R. C. Elphic, Initial ISEE magnetometer results: Magnetopause observations, *Space Sci. Rev.*, 22, 681, 1978.
- Russell, C. T., J. G. Luhmann, T. J. Odera, and W. F. Stuart, The rate of occurrence of dayside PC 3,4 pulsations: The L-value dependence of the IMF cone angle effect, *Geophys. Res. Lett.*, 10, 663, 1983.
- Saito, T., A new index of geomagnetic pulsations and its relation to solar M-region, Part 1, *Rep. Ionos. Space Res., Japan*, 18, 260, 1964.
- Saito, T., and S. Matsushita, Geomagnetic pulsations associated with sudden commencements and sudden impulses, *Planet. Space Sci.*, 15, 573, 1967.
- Saito, T., K. Yumoto, K. Takahashi, T. Tamura, and T. Sakurai, Solar wind control of Pc 3, Magnetospheric Study 1979, in *Proceedings of International Workshop on Selected Topics of Magnetospheric Physics*, p155, Japanese IMS Committee, Tokyo, 1979.
- Song, P., R. C. Elphic, and C. T. Russell, ISEE 1 and 2 observations of the oscillating magnetopause, *Geophys. Res. Lett.*, 15, 744, 1988.
- Spreiter, J. R., and A. Y. Alksne, Plasma flow around the magnetosphere, *Rev. Geophys.*, 7, 11, 1969.
- Takahashi, K., R. L. McPherron, E. W. Greenstadt, and C. A. Neeley, Factors controlling the occurrence of Pc 3 magnetic pulsations at synchronous orbit, *J. Geophys. Res.*, 86, A7, 5472, 1981.
- Tomomura, K., T. Sakurai, and Y. Kato, Satellite observation of magnetic fluctuations in the magnetosheath and the magnetosphere, *Proc. Faculty Eng.*, 9, Tokai Univ., 1983.
- Troitskaya, V. A. and O. V. Bol'shakova, The relation of the high-latitude maximum of Pc3 intensity to the dayside cusp, *Geomag. and Aeron.*, 7, 633, 1984.
- Troitskaya, V. A., Y. A. Plyasova-Bakunina, and A. V. Gul'yel'mi, Relationship between Pc 2-4 pulsations and the interplanetary magnetic field, *Dokl. Akad. Nauk. SSSR*, 197, 1312, 1971.
- Vero, J. and L. Hollo, Connections between interplanetary magnetic field and geomagnetic pulsations, *J. Atmos. Terr. Phys.*, 40, 857, 1978.
- Verzariu, P., Reflection and refraction of hydromagnetic waves at the magnetopause, *Planet. Space Sci.*, 21, 2213, 1973.
- Vinogradov, P. A., and V. A. Parkhomov, MHD waves in the solar wind—a possible source of geomagnetic Pc3 pulsations, *Geomagn. Aeron.*, 15, 109, 1974.
- Walker, R. J., T. Ogino, and M. Ashour-Abdalla, Simulating the magnetosphere: The structure of the magnetotail, *Solar System Plasma Physics, AGU Monograph 54*, J. H. Waite, J. L. Burch, and R. L. Moore, eds., 61, 1989.
- Wolfe, A., Dependence of mid-latitude hydromagnetic energy spectra on solar wind speed and interplanetary field direction, *J. Geophys. Res.*, 85,
- Wolfe, A., and R. L. Kaufmann, MHD wave transmission and production near the magnetopause, *J. Geophys. Res.*, 80, 1764, 1975.
- Wolfe, A., L. J. Lanzerotti, and C. G. MacLennan, Dependence of hydromagnetic energy spectra on solar wind velocity and interplanetary magnetic field direction, *J. Geophys. Res.*, 85, 114, 1980.
- Wolfe, A., C. Uberoi, C. T. Russell, L. J. Lanzerotti, C. G. MacLennan, and L. V. Medford, Penetration of hydromagnetic wave energy deep into the magnetosphere, *Planet. Space Sci.*, 39, 1317, 1989.
- Yumoto, I., and T. Saito, Relation of compressional HM waves at GOES 2 to low-latitude Pc 3 magnetic pulsations, *J. Geophys. Res.*, 88, 10041, 1983.
- Yumoto, K., T. Saito, B. T. Tsurutani, E. J. Smith, and S-I Akasofu, Relationship between the IMF magnitude and Pc 3 magnetic pulsations in the magnetosphere, *J. Geophys. Res.*, 89, 9731, 1984.

## FIGURE CAPTIONS

Fig. 1. Distributions of various measures of wave activity across local daylight longitudes recorded by Explorer 34, in the magnetosheath; at Kakioka magnetic observatory; and at Resolute Bay and Baker Lake magnetic observatories. The panels document the tendency of daytime pulsations to peak in amplitude and Pc3,4 frequencies around midmorning to midday.

Fig. 2. Scatter diagrams showing weak, but consistent correlations of Pc3,4 occurrence and amplitude at Earth's surface with IMF cone angle,  $a$ , and solar wind speed,  $b$ . Top of  $a$ , hourly occurrence probability of Pc3 at Onagawa vs. cone angle  $\theta_{XB}$  [Saito et al., 1979]; bottom of  $a$ , hourly maximal amplitude of Pc4 at Calgary vs.  $\cos(\theta_{XB})$  [Greenstadt and Olson, 1977]. Top of  $b$ , hourly occurrence probability of Pc3 at Onagawa vs. solar wind speed  $V_{SW}$  [Saito et al., 1979]; bottom left of  $b$ , hourly maximal amplitude of Pc4 at Calgary vs.  $V_{SW}$  [Greenstadt et al., 1979]; bottom right, amplitude in three-hour intervals of Pc3 for  $20 < T < 40$  s at Petropavlovsk-Kamchatsky vs.  $V_{SW}$  [Kovner et al., 1976].

Fig. 3. Two sketches of the magnetosphere in the noon-meridian plane at equinox (E, upper right) and summer solstice (SS, lower right), and a diagram of the annual cycles of the magnetic pole's orientation with respect to the solar wind flow from the sun, (left center). Arrows in the right hand sketches indicate the solar wind direction; shaded curves show approximate flow lines in the magnetosheath that cross the terminator at about  $1 R_E$  from the magnetopause.

Fig. 4. Two sketches of the extreme patterns of ULF activity in the subsolar magnetosheath, when the IMF is parallel (or antiparallel) to the solar wind flow, at left; and in the flanks when the IMF is across the flow, at right.

Fig. 5. Projections of boundaries between  $Q_{\perp}$  (clear) and  $Q_{\parallel}$  (shaded) regions of Earth's bow shock for various IMF cone angle ( $\theta_{XB}$ ) orientations;  $a$  and  $b$  present X-Y and Y-Z meridian projections for  $\theta_{XB} = 45^\circ$ ;  $c$  and  $d$  present Y-Z projections for  $\theta_{XB} = 30^\circ$  and  $60^\circ$ . In  $a$  and  $b$  lighter shading indicates a region of alternating  $Q_{\perp}$  and  $Q_{\parallel}$  shock structures according to variable  $\theta_{Bn}$  between the IMF and the local shock normal  $n$  introduced by large amplitude foreshock waves impinging on the bow shock.

Fig. 6. X-Y and Y-Z projections of Earth's bow shock for rough subdivisions of  $\theta_{XB} = 45^\circ$ , with variable shading showing rough subdivisions of  $Q_{\perp}/Q_{\parallel}$  structure of the shock and, by implication, the magnetosheath, in relation to the solar wind flow tube that encloses the magnetopause.

Fig. 7. Examples of the highly replicable linkage  $f \sim 6B$  between geomagnetic pulsation frequency and IMF magnitude. Upper three panels: scatter diagrams for geosynchronous and surface observations at



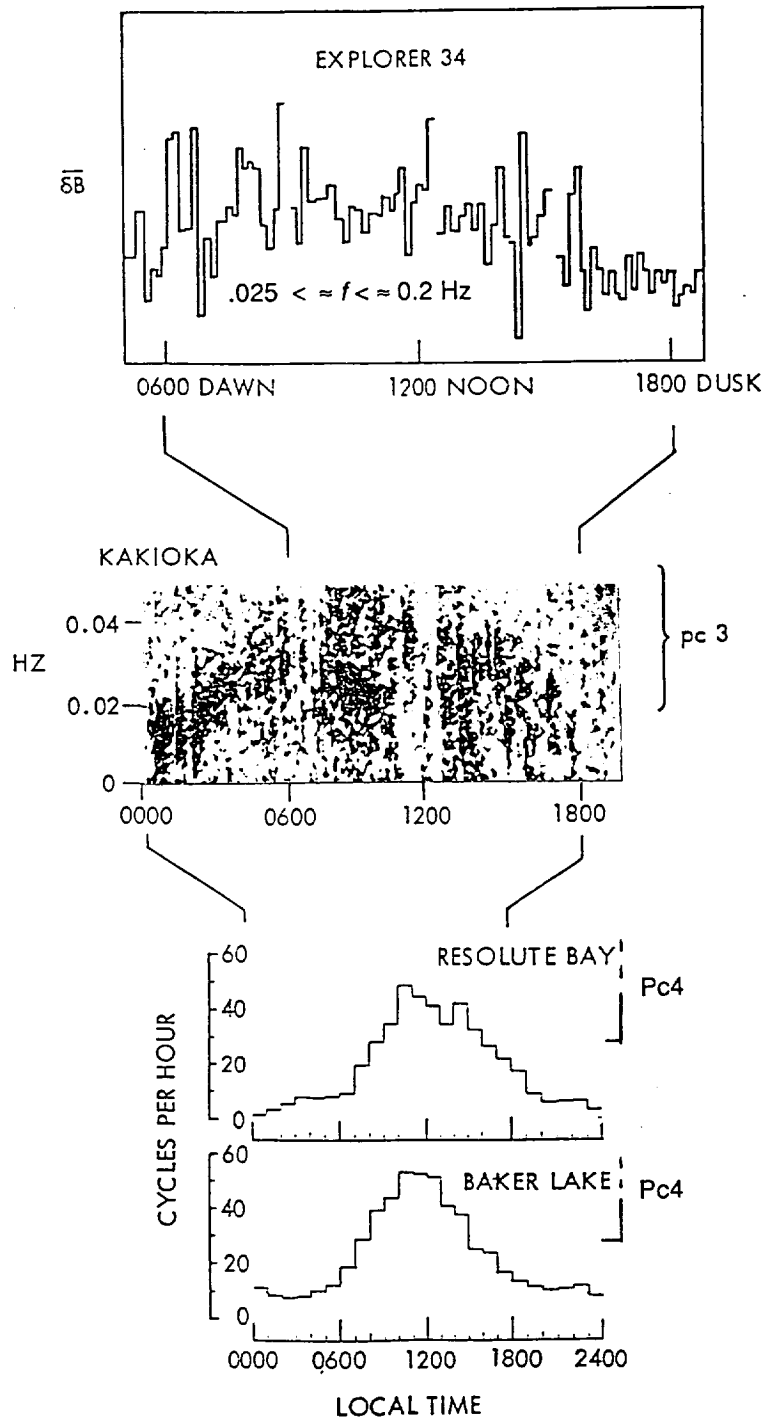


Fig. 1. Distributions of various measures of wave activity across local daylight longitudes recorded by Explorer 34, in the magnetosheath; at Kakioka magnetic observatory; and at Resolute Bay and Baker Lake magnetic observatories. The panels document the tendency of daytime pulsations to peak in amplitude and Pc3,4 frequencies around midmorning to midday.

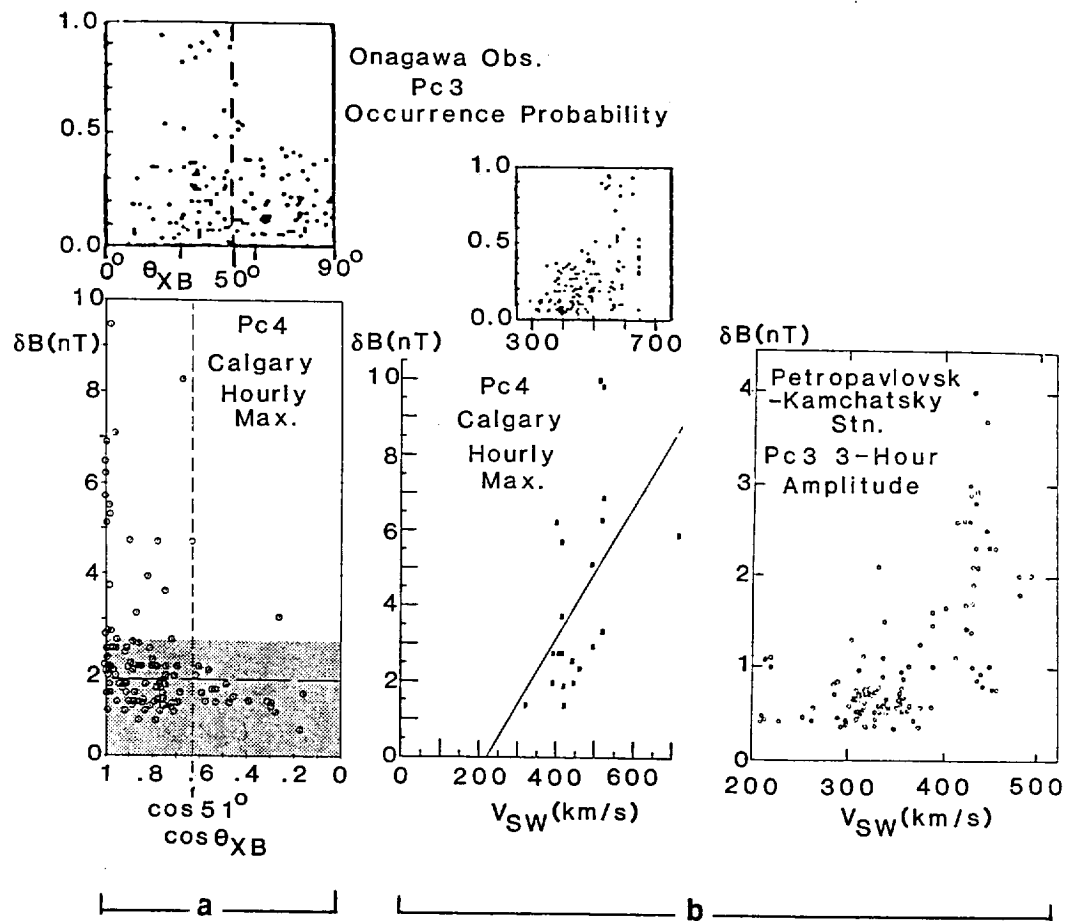


Fig. 2. Scatter diagrams showing weak, but consistent correlations of Pc3,4 occurrence and amplitude at Earth's surface with IMF cone angle,  $a$ , and solar wind speed,  $b$ . Top of  $a$ , hourly occurrence probability of Pc3 at Onagawa vs. cone angle  $\theta_{XB}$  [Saito et al., 1979]; bottom of  $a$ , hourly maximal amplitude of Pc4 at Calgary vs.  $\cos(\theta_{XB})$  [Greenstadt and Olson, 1977]. Top of  $b$ , hourly occurrence probability of Pc3 at Onagawa vs. solar wind speed  $V_{SW}$  [Saito et al., 1979]; bottom left of  $b$ , hourly maximal amplitude of Pc4 at Calgary vs.  $V_{SW}$  [Greenstadt et al., 1979]; bottom right, amplitude in three-hour intervals of Pc3 for  $20 < T < 40$  s at Petropavlovsk-Kamchatsky vs.  $V_{SW}$  [Kovner et al., 1976].

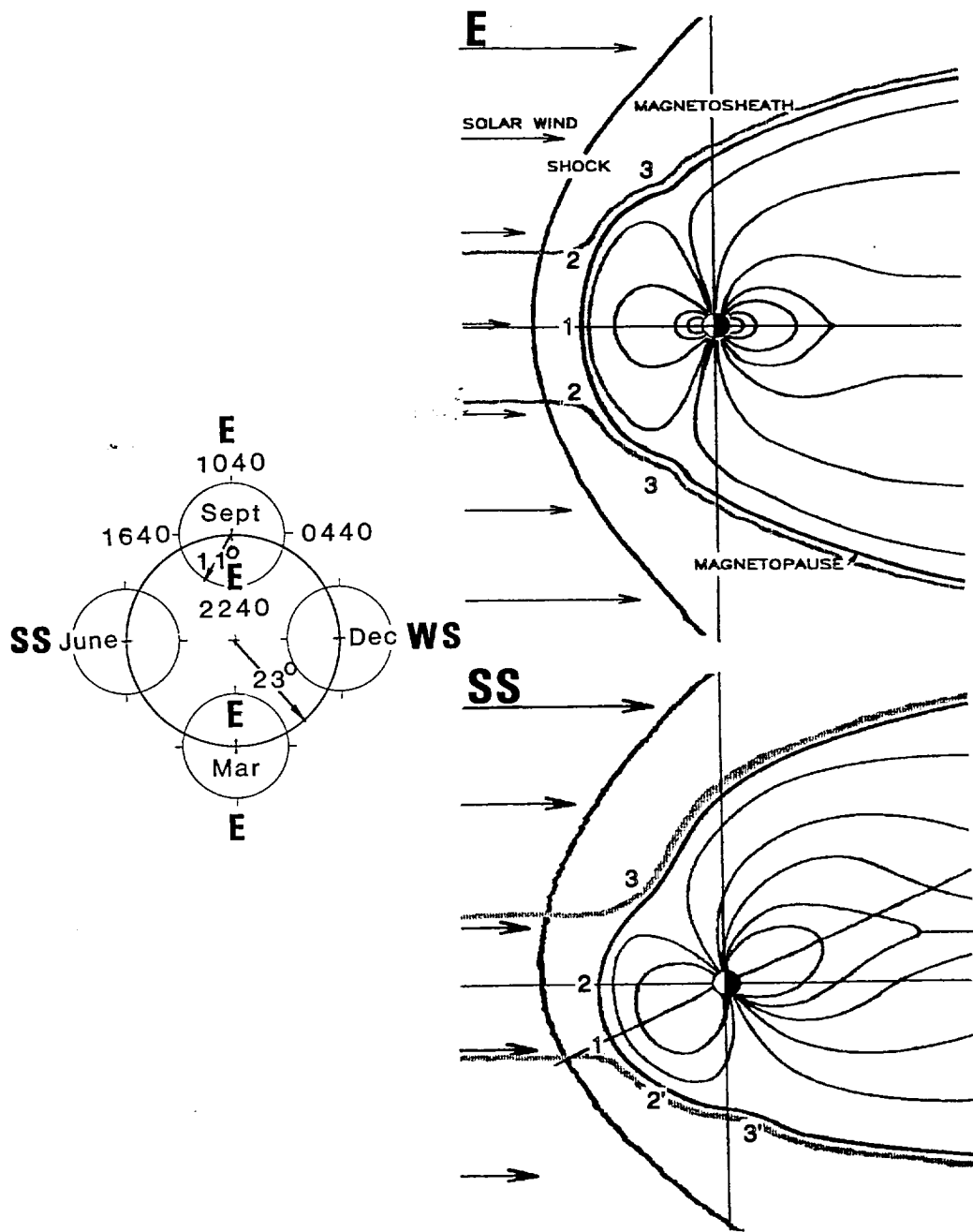


Fig. 3. Two sketches of the magnetosphere in the noon-meridian plane at equinox (E, upper right) and summer solstice (SS, lower right), and a diagram of the annual cycles of the magnetic pole's orientation with respect to the solar wind flow from the sun, (left center). Arrows in the right hand sketches indicate the solar wind direction; shaded curves show approximate flow lines in the magnetosheath that cross the terminator at about  $1 R_E$  from the magnetopause.

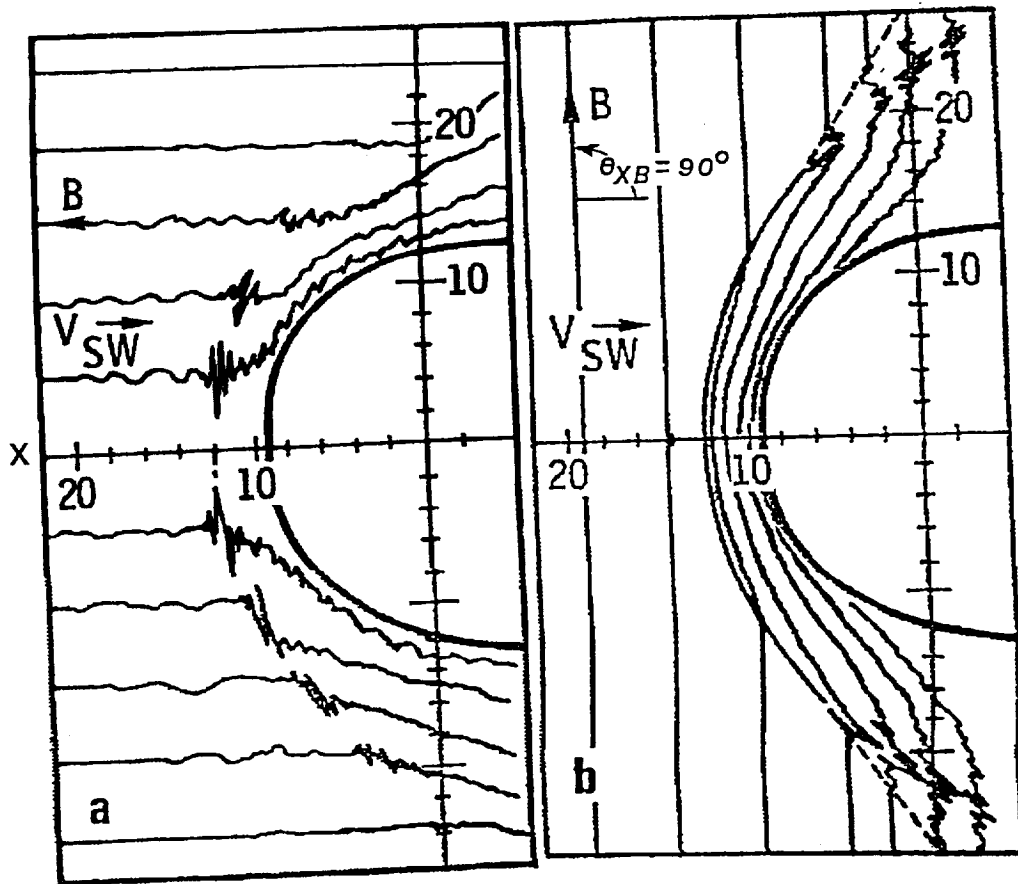


Fig. 4. Two sketches of the extreme patterns of ULF activity in the subsolar magnetosheath, when the IMF is parallel (or antiparallel) to the solar wind flow, at left; and in the flanks when the IMF is across the flow, at right.

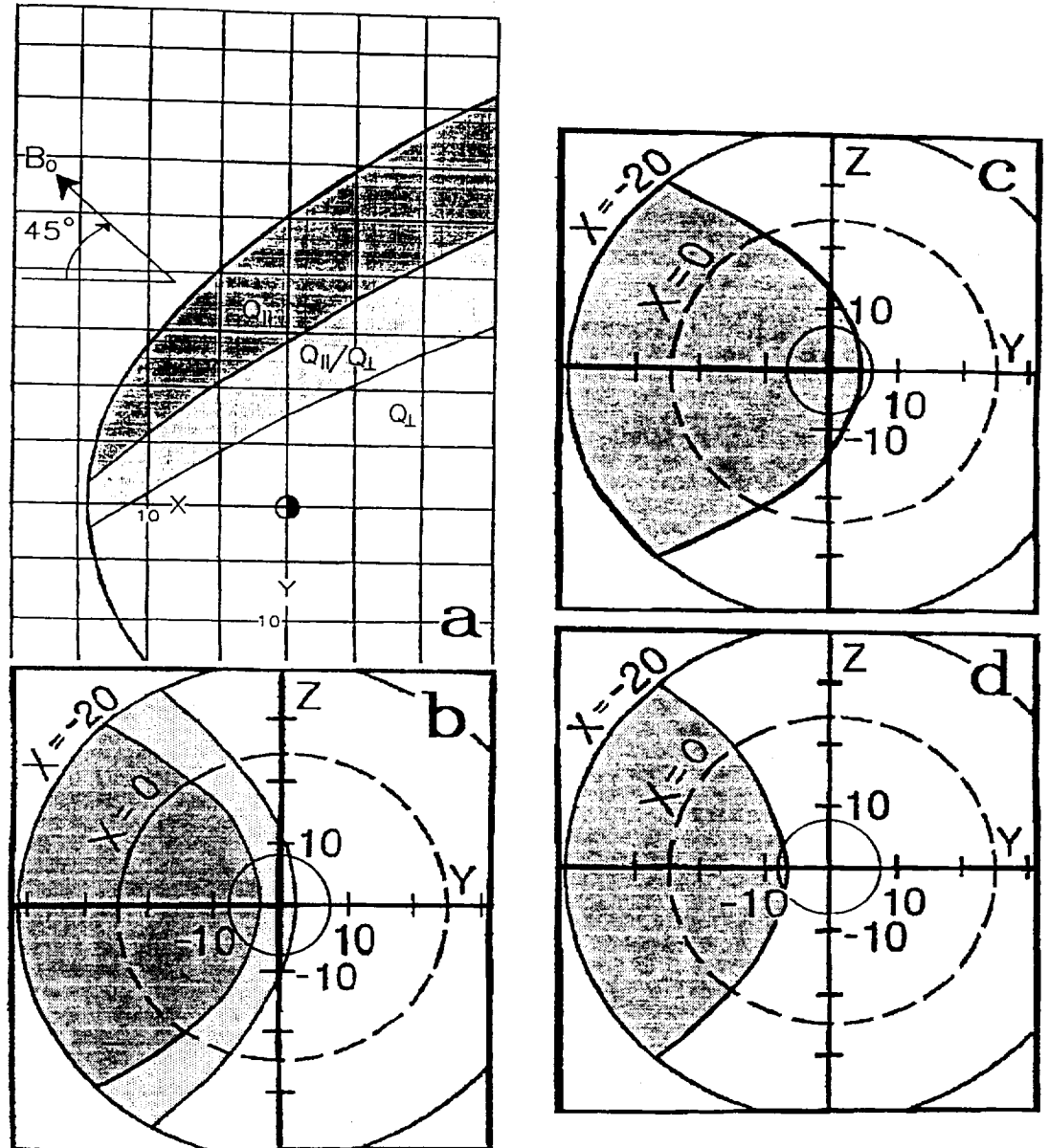


Fig. 5. Projections of boundaries between  $Q_{\perp}$  (clear) and  $Q_{\parallel}$  (shaded) regions of Earth's bow shock for various IMF cone angle ( $\theta_{XB}$ ) orientations; a and b present X-Y and Y-Z meridian projections for  $\theta_{XB} = 45^\circ$ ; c and d present Y-Z projections for  $\theta_{XB} = 30^\circ$  and  $60^\circ$ . In a and b lighter shading indicates a region of alternating  $Q_{\perp}$  and  $Q_{\parallel}$  shock structures according to variable  $\theta_{Bn}$  between the IMF and the local shock normal  $n$  introduced by large amplitude foreshock waves impinging on the bow shock.

$$\theta_{XB} = 45^\circ \quad \theta_{Bn} = 51^\circ$$

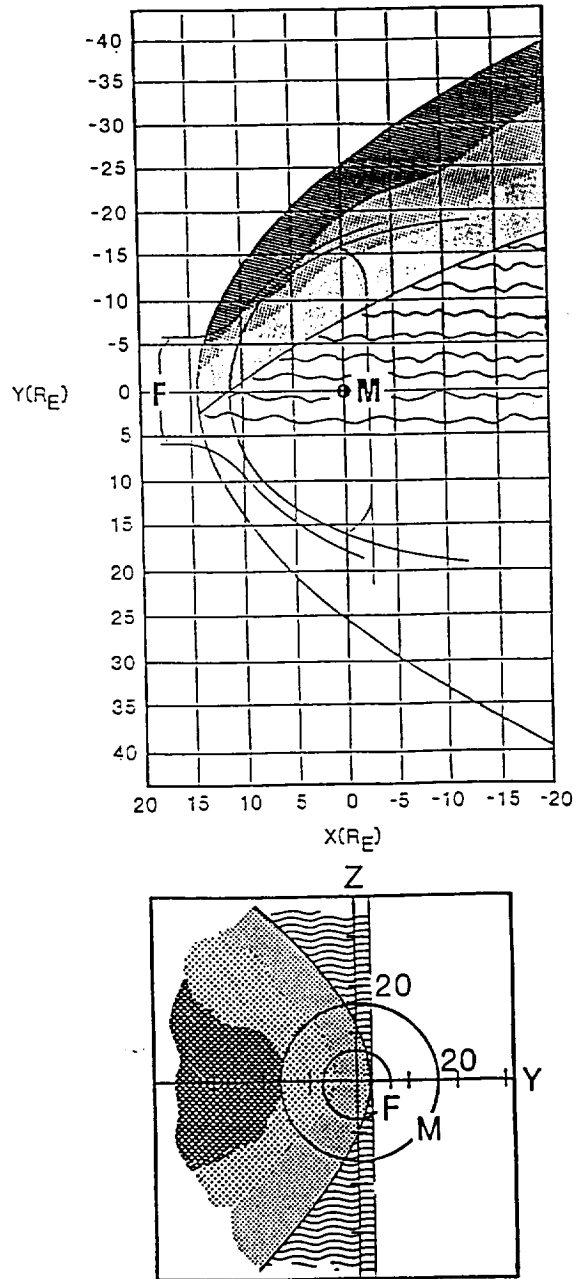
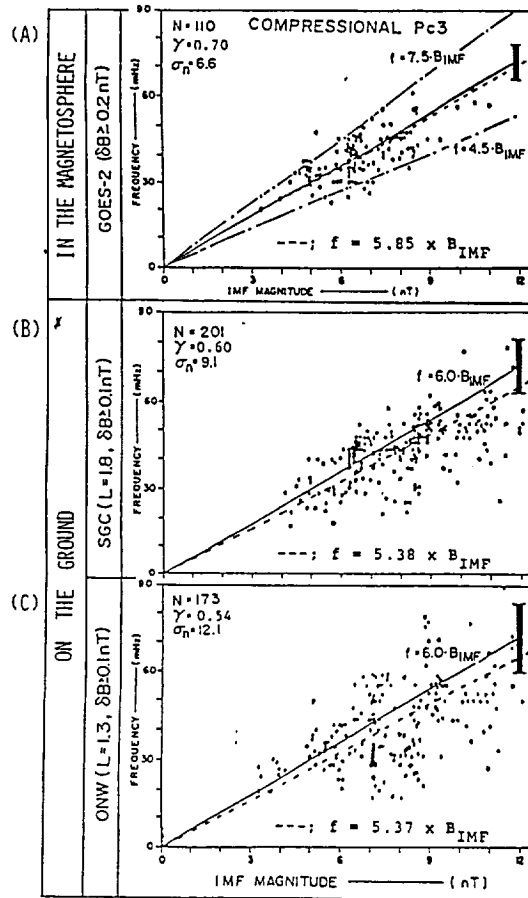


Fig. 6. X-Y and Y-Z projections of Earth's bow shock for rough subdivisions of  $\theta_{XB} = 45^\circ$ , with variable shading showing rough subdivisions of  $Q_{\perp}/Q_{\parallel}$  structure of the shock and, by implication, the magnetosheath, in relation to the solar wind flow tube that encloses the magnetopause.

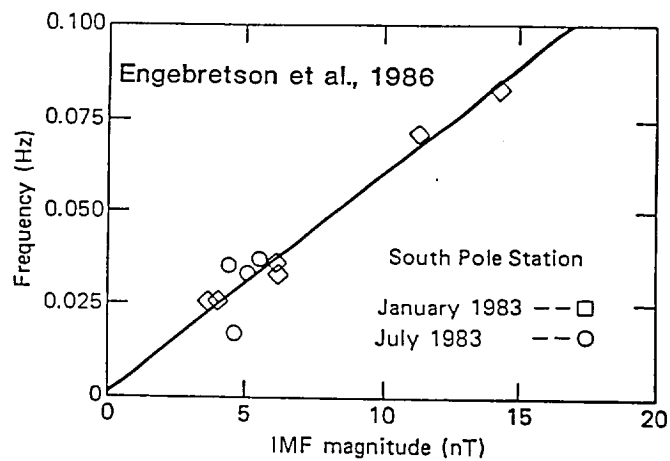
Yumoto et al., 1984



GEOSYNCH

L 1.8

L 1.3



CUSP

Fig. 7. Examples of the highly replicable linkage  $f \sim 6B$  between geomagnetic pulsation frequency and IMF magnitude. Upper three panels: scatter diagrams for geosynchronous and surface observations at low magnetic latitudes; bottom panel: measurements at a station connected to a polar lobe at higher latitude than the auroral zone.

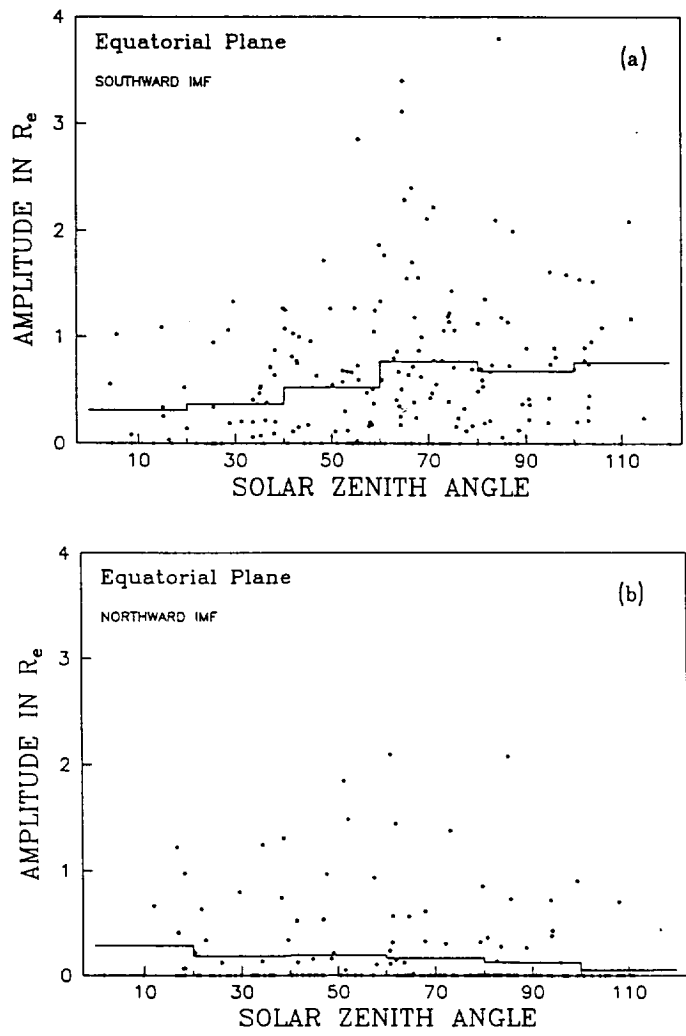


Fig. 8. Amplitude of magnetopause oscillation vs. solar zenith angle near the equatorial plane. The data are within  $\pm 30^\circ$  of the GSM equatorial plane. The solid line is the mean value, a) When the IMF is southward, b) When the IMF is northward.

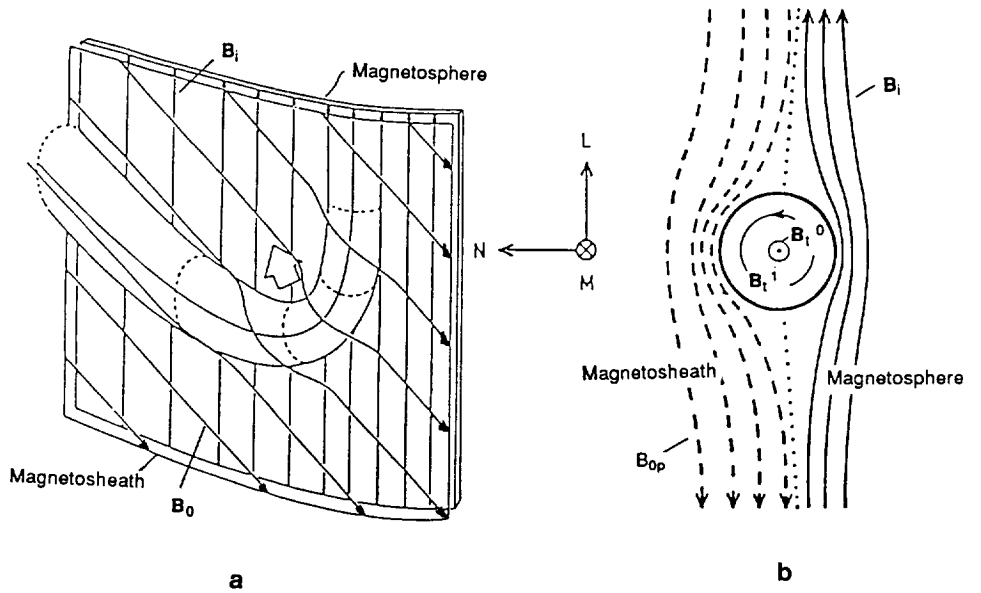


Fig. 9. The distortion of the magnetosheath and magnetospheric magnetic fields by a flux transfer event. The left hand panel shows the view from the magnetosheath. The right hand panel shows a cross-section of the magnetopause [after Russell and Elphic, 1978; Cowley, 1982].

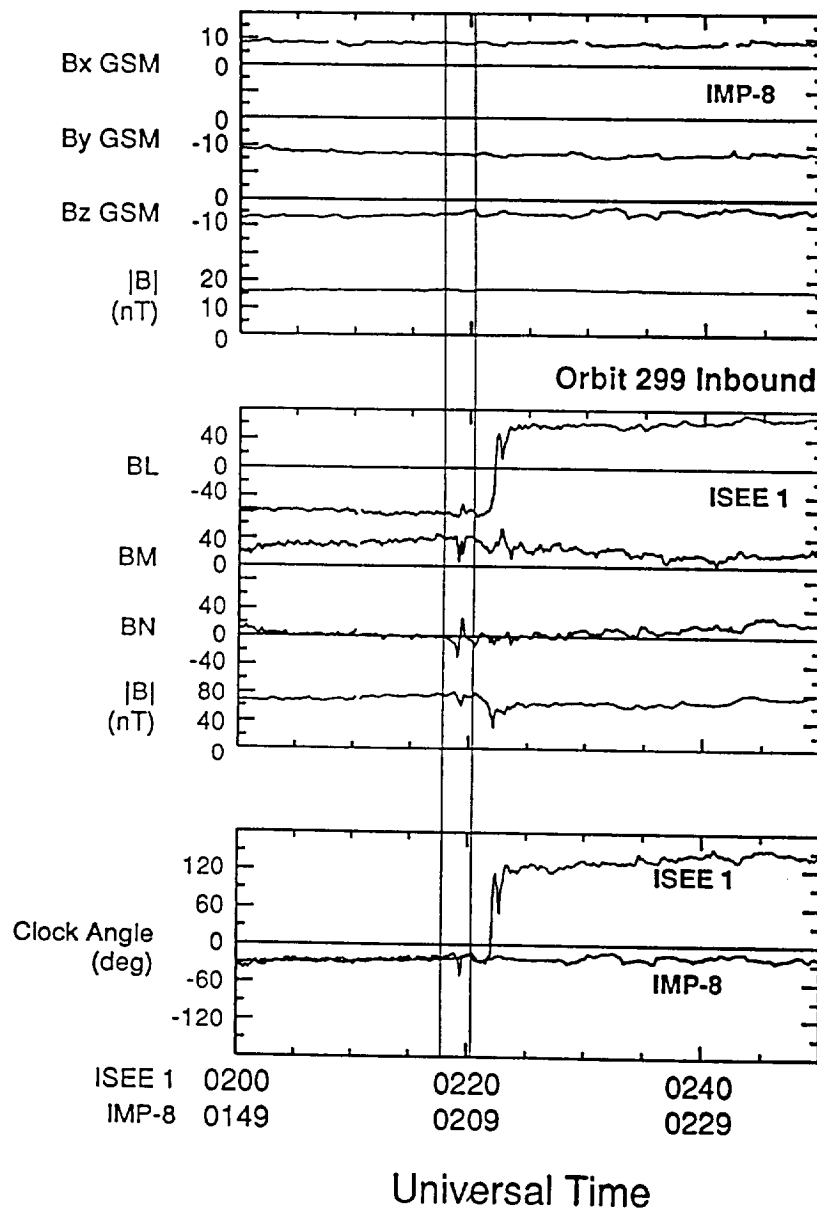


Fig. 10. Interplanetary conditions during FTE occurrence showing that FTEs are not triggered by fluctuations in the IMF. Top panel shows the IMF measured at IMP 8. The middle panel shows the magnetic field measured by ISEE 1 as it moved from the magnetosheath to the magnetosphere. The bottom panel shows the clock angle of the IMF about the solar direction and at ISEE 1 have the same clock angle except at the FTE and after the crossing of the magnetopause. The steadiness of the IMF B vector around the time of the FTE indicates that there was no FTE trigger in the solar wind, but that the FTE arose spontaneously at the magnetopause during southward IMF.

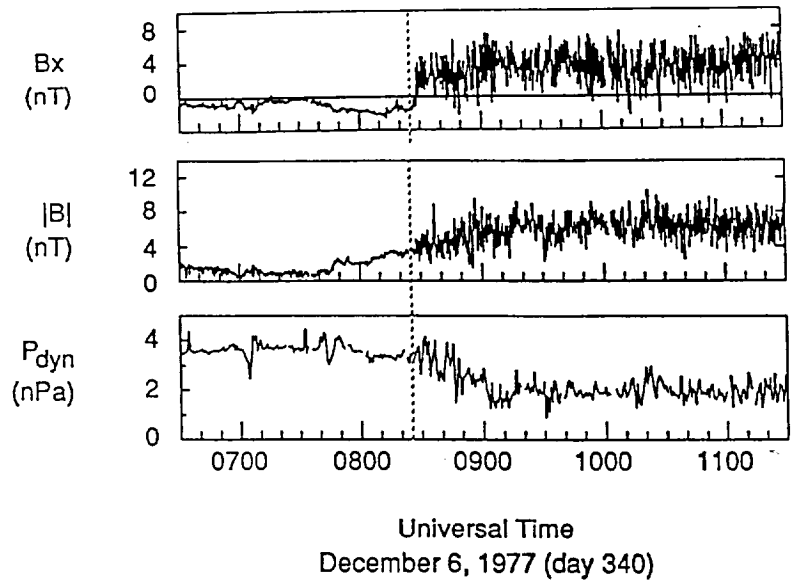


Fig. 11. Three panels from Figure 3.6 of Le [1991] showing a drop in solar wind pressure following entry of the foreshock (dotted line) that accompanied a sudden shift in direction of the IMF, synopsisized by  $B_x$  in the top panel.

# MAGNETIC AND ELECTRIC FIELD WAVES IN SLOW SHOCKS OF THE DISTANT GEOMAGNETIC TAIL: ISEE 3 OBSERVATIONS

F. V. Coroniti, S. L. Moses, and E. W. Greenstadt  
*TRW Space and Electronics Group, Redondo Beach CA*

B. T. Tsurutani and E. J. Smith  
*California Institute of Technology, Jet Propulsion Laboratory, Pasadena CA*

**Abstract.** During ISEE 3's first pass through the distant geomagnetic tail, the slow shocks encountered on February 2 and 11, 1983 provide particularly clear examples of the magnetic field and plasma wave properties of the shock transition. The magnetic ramp contains transverse polarized magnetic field oscillations with frequencies just below the ion cyclotron frequency and amplitudes of 2 to 4 nT. These waves are plausibly generated by the electromagnetic ion/ion cyclotron instability predicted by *Winske and Omidi* [1990]. The electric field plasma waves within the shock ramp exhibit two spectral peaks. A mid-frequency emission occurs near the ion plasma frequency and electron cyclotron frequency, but well below the maximum Doppler shift frequency for electrostatic waves. The mid-frequency waves extend into the upstream region where the spectral peak occurs at a slightly higher frequency. A new high frequency emission with frequencies between the maximum Doppler shift frequency and the electron plasma frequency occurs throughout the downstream region. This emission disappears at the start of the magnetic ramp, and is replaced upstream by electron plasma oscillations. The high frequency emissions are clearly polarized parallel to the magnetic field. The polarization of the mid-frequency waves is less certain; both parallel and a fairly broad angular distribution about the parallel electric fields are consistent with the measurements.

## 1. Introduction

The ISEE 3 passes through the distant geomagnetic tail provided the first identification of slow shocks which hydromagnetic models of reconnection predict should stand in the upstream flow and bound the plasma sheet [*Feldman et al.*, 1984, 1985]. As in fast mode shocks, plasma wave turbulence occurs in both the upstream and downstream regions of the distant tail slow shocks [*Scarf et al.*, 1984]. Within the slow shock's magnetic ramp and extending into the upstream flow, the electric field wave emissions exhibit a relatively narrowband peak near, but usually above, the ion plasma frequency which resembles the waves detected in fast shocks [*Gurnett,*

1985]. Upstream, electron plasma oscillations often occur in association with the heat flux carried by shock-heated electrons escaping along the magnetic field lines. A search for lower hybrid emissions, which are potential sources of anomalous resistance, failed to detect the magnetic component of these waves [Coroniti *et al.*, 1988].

The previous studies of waves in the slow shocks emphasized the average spectral characteristics of the emissions; neither the high time resolution structure of the slow shock electric or magnetic field waves, nor the electric field polarization were investigated. In this paper we carry out these heretofore neglected investigations. Section 2 discusses the average E-field spectral changes which occurred during two ISEE 3 slow shock encounters in February, 1983. In Section 3 we present high time resolution magnetic field and plasma wave measurements. Large amplitude nearly transverse magnetic field perturbations occur within the magnetic field shock ramp. The mid-frequency, narrowband plasma waves are highly impulsive, and occur both in the upstream and downstream regions. We also identify a new high frequency wave mode which occurs in the magnetic ramp, but disappears in the upstream region. Section 4 discusses the electric field polarization characteristics, and Section 5 offers some comments on these measurements.

## 2. Slow Shock Spectra

The two slow shocks occurred on February 2 and 11, 1983 when ISEE 3 was located in the distant tail about 220  $R_E$  downstream. The upstream and downstream plasma parameters for these shocks are given in *Feldman et al.* [1985] and *Schwartz et al.* [1987]; both shocks had Alfvén Mach numbers and propagation angles to the upstream field that correspond to nearly switch-off slow shock conditions. For the February 2 shock the upstream (downstream) plasma density, electron temperature, flow speed, and magnetic field strength are  $n_1 = 0.3 \text{ cm}^{-3}$  ( $n_2 = 0.5 \text{ cm}^{-3}$ ),  $T_{e1} = 3.3 \times 10^5 \text{ K}$  ( $T_{e2} = 8 \times 10^5 \text{ K}$ ),  $v_{x1} = 210 \text{ km/s}$  ( $v_{x2} = 530 \text{ km/s}$ ), and  $B_1 = 10.8 \text{ nT}$  ( $B_2 = 3 \text{ nT}$ ). For the February 11 shock the corresponding parameters are  $n_1 = 0.27 \text{ cm}^{-3}$  ( $n_2 = 0.750 \text{ cm}^{-3}$ ),  $T_{e1} = 7 \times 10^5 \text{ K}$  ( $T_{e2} = 1.8 \times 10^6 \text{ K}$ ),  $v_{x1} = 90 \text{ km/s}$  ( $v_{x2} = 750 \text{ km/s}$ ), and  $B_1 = 19 \text{ nT}$  ( $B_2 = 4 \text{ nT}$ ). The downstream ion temperatures inferred from pressure balance between the upstream field strength and downstream plasma pressure is  $T_{i2} = 0.6 \text{ keV}$  ( $T_{i2} = 1.25 \text{ keV}$ ) for the February 2 (11) shocks.

In the discussion below we refer to the following characteristic wave frequencies;  $f_c = 28 B(\text{nT})\text{Hz}$  is the electron cyclotron frequency;  $f_{pe} = 9 n^{1/2} \text{ kHz}$  is the electron plasma frequency; and  $f_{pi} = 210 n^{1/2} \text{ Hz}$  is the ion plasma frequency for hydrogen. The lower hybrid frequency is typically below the lowest electric field frequency channel (17.8 Hz) of the TRW/U. Iowa plasma wave

detector. The maximum Doppler shift frequency for a wave with wave number  $k$  is  $f_D = k\lambda_D (v/v_e)f_{pe}$  where  $v = v_x$  is the flow speed,  $v_e = (T_e/m_e)^{1/2}$  and  $\lambda_D = v_e/(2\pi f_{pe})$  is the Debye length.

### *Slow Shock on February 2, 1983*

Figure 1 displays nine selected peak (top curves) and 30-second average (bottom curves) electric field amplitude spectra (volts/m-Hz<sup>1/2</sup>) for the February 2, 1983 slow shock. For reference the magnetic field strength ( $B$ ) and the x-component ( $B_x$ ) are shown in the center; detailed field profiles can be found in *Coroniti et al.* [1988]. The three bottom spectra were obtained between 1924:37 UT to 1935:00 UT when the spacecraft was in the region upstream of the shock. The narrow peaked emissions at 5.6 kHz are electron plasma oscillations which are presumably excited by shock-heated electrons that escape upstream. The plasma oscillations terminate at 1947 UT when the escaping electron heat flux abruptly decreased [*Feldman et al.*, 1985]. In the mid-frequency range (50 - 500 Hz), the spectra exhibit a strong peak near 178 - 316 Hz; in contrast to the broad power law spectra of broadband electrostatic noise (BEN) [*Gurnett et al.*, 1976; *Grabbe and Eastman*, 1984] this mid-frequency emission has been termed narrowband electrostatic noise (NEN) [*Coroniti and Ashour-Abdalla*, 1989]. The NEN peak is above the upstream ion plasma frequency ( $f_{pi} = 115$  Hz), and near, but below, the upstream electron cyclotron frequency ( $f_c = 300$  Hz). The upstream Doppler frequency is  $f_D = 460 k\lambda_D$  Hz. The upstream NEN also continues to 1947 UT, and diminishes with the decrease in the electron heat flux.

The 1922:27 UT spectrum was obtained midway through the magnetic shock ramp. The electron plasma oscillations have disappeared, and a slight amplitude enhancement has developed between 1.78 and 5.6 kHz. In the 1920:50 UT spectrum taken at the bottom of the ramp, this slight enhancement has become a definite second peak in both the average and peak spectra, and this high-frequency emission is clearly separated from the mid-frequency NEN peak by a break or dip in the spectral slope. The maximum of the NEN now occurs between 100 and 178 Hz, but is clearly below the peak frequency of the upstream NEN. At 1920:50 the characteristic wave frequencies are  $f_{pi} = 150$  Hz,  $f_c = 140$  Hz and  $f_D = 730 k\lambda_D$  Hz.

The 1919:12 UT spectrum was obtained just before the start of the shock ramp, on the plateau in magnetic field strength ( $B = 3$  nT); the field strength is about equally divided between the  $B_x$  and  $B_y$  components. Both the NEN and high frequency peaks have decreased, but are still clearly discernable. At 1917:02 UT, the NEN spectral peak has disappeared, but the high frequency emission is still present. Although the field strength remains near 3 nT,  $B_x$  is nearly zero, and the

total field is carried by the  $B_y$  component. The vanishing of  $B_x$  corresponds to the downstream state of the switch-off shock. Finally, the 1914:20 UT spectrum was obtained on the other side of the  $B_x$  reversal ( $B_x < 0$  to  $B_x > 0$ ), but still on the magnetic plateau. The high frequency and NEN spectral peaks are at frequencies of 3.16 kHz and 178 Hz, respectively, and the break in spectral slope between the two emissions occurs at 1 kHz, which equals the maximum Doppler shift frequency for waves with  $k\lambda_D = 1$ .

### *Slow Shock on February 11, 1983*

Figure 2 displays selected frequency spectra and the magnetic field ( $B$  and  $B_x$ ) for the slow shock encountered at 2025 to 2030 UT on February 11, 1983. The 2031:05 UT spectra exhibits the upstream plasma oscillation peak at 5.6 kHz and the NEN peak near 178 - 316 Hz. The upstream ion plasma frequency was  $f_{pi} = 110$  Hz, whereas the electron cyclotron frequency was  $f_c = 540$  Hz, which is well above the NEN peak. In the 2028:5 UT spectrum measured at the start of the magnetic ramp, the electron plasma oscillations have disappeared, and a weak peak has developed between 1.78 and 3.16 kHz. At the base of the magnetic ramp (2027:50 UT spectrum) this high frequency emission clearly extends from 1 kHz to at least 10 kHz. The maximum Doppler shift frequency is  $1.1 k\lambda_D$  kHz, and the downstream electron plasma frequency is 7.8 kHz; thus the high frequency emission cannot simply be the result of Doppler up-shifting of low frequency waves. The NEN amplitudes maximize between 100 Hz and 178 Hz which is lower than the NEN upstream peak frequency; the NEN frequencies are still below the local electron cyclotron frequency (approximately 280 Hz) but are now comparable to the downstream ion plasma frequency.

The mid- and high frequency components persist in the downstream flow and are still discernable (2022:57 UT spectrum) after the magnetic field strength decreases to 4.5 nT (2025 UT). The NEN spectral peak remains near 100-178 Hz, and is now close to the local electron cyclotron frequency. At 2022:25 UT, both  $B_x$  and  $B_y$  are nearly zero, and the field magnitude is carried by the  $B_z = -4$  nT component. In the 2022:25 UT spectrum, the NEN peak has disappeared and the high frequency emission is barely (if at all) perceptible.

### *Discussion*

Downstream of the leading edge decrease in the magnetic field, the wave spectra in both slow shocks exhibit distinct mid- and high frequency peaks. A spectral break separates the two emissions and the frequency of the break is close to the maximum Doppler shift frequency for

modes with  $k\lambda_D = 1$ . The spectra of these two emissions strongly resemble the wave spectra detected downstream of the low Mach number fast shocks on the flanks of the magnetosphere [Coroniti *et al.*, 1993]. In both the fast and slow shock spectra, the high frequency signals start near  $f_D$  and extend up to the local electron plasma frequency; we show below that the high frequency modes in the slow shocks are also polarized along the magnetic field.

In the weak flank bow shocks, the mid-frequency waves occurred at frequencies well above the downstream electron cyclotron frequency, near or just above the ion plasma frequency, and well below the maximum Doppler shift frequency; however, the downstream plasma and magnetic field values did not vary greatly for the fast shocks studied by Coroniti *et al* [1993]. For the two February 1983 slow shocks, the upstream NEN spectral peak was close to the local electron cyclotron frequency for one shock, but well below  $f_c$  for the other; in both cases the peak was above the upstream ion plasma frequency. Downstream the NEN peak occurs at a lower frequency, and is close to both  $f_c$  and  $f_{pi}$ . Since  $f_{pi}$  increases across the slow shock, the NEN peak frequency does not scale (in any obvious way) with density. The peak frequency could scale with magnetic field strength; however, since the two slow shocks had quite different upstream field strengths but the same NEN spectral peak frequencies, the emission is apparently not controlled (at least significantly) by the magnetic field strength. Curiously, in both slow shocks, the mid-frequency emission disappears when  $B_x$  vanishes, even though the magnetic field strength remained constant during the  $B_x$  sign reversal interval.

Finally, the peak NEN frequency is clearly anti-correlated with the maximum Doppler shift frequency, which increases strongly from upstream to downstream in the slow shock. The anti-correlation suggests that the mid-frequency signals are not significantly Doppler shifted. There are (at least) two possible ways to avoid Doppler shifting. Firstly, if the wavelengths are so long that  $f_D \ll f$ , the measured mode frequencies will be unaffected by the flow. For the downstream NEN,  $f_D \ll f$  requires  $k\lambda_D < 1/10 - 1/20$ . The second possibility is that the waves do not couple to the bulk ion flow, but, for example, only to the electron species; the electron velocity space hole modes proposed by Coroniti and Ashour-Abdalla [1989] and very cold fast ion beam modes [Grabbe and Eastman, 1984] have this property, but ion acoustic waves do not. The mid-frequency waves detected in the magnetosheath, which spectrally resemble NEN, have measured or inferred wavelengths of  $k\lambda_D = 0.1 - 1.0$  [Rodriquez, 1979; Anderson *et al.*, 1982; Gallagher, 1985], and are usually assumed or inferred to be ion acoustic waves [Gallagher, 1985]. Whether the magnetosheath emissions and NEN are physically related is, however, undetermined.

### 3. High Time Resolved Slow Shock Structure

### *February 2, 1983 Slow Shock*

Figures 3 a,b,c display the magnetic field at the highest time resolution of 1/6 second per vector and the plasma wave E-Field amplitudes measured every 0.5 second for the ramp interval of the February 2, 1983 slow shock. From 1918 to 1919 UT (Figure 3a)  $B_x$  and  $B_z$  are near zero, and the 3 to 4 nT field strength is carried in the  $B_y$  component; just before 1918  $B_x$  changed sign (to positive), so that the  $B_x$  near zero period after 1918 UT would represent the downstream end of the slow shock transition. The mid-frequency wave signals are very weak, and the high frequency intensities are low but clearly present. At 1918:40 UT oscillations began in  $B_z$ . The mid-frequency wave amplitudes abruptly increased at 1919 UT just when the magnetic field strength started to increase in the ramp. During the next minute, the bursts of mid-frequency emissions became more frequent so that after 1920 UT these signals are nearly continuous although temporally impulsive. The high frequency waves exhibit a clear modulation of the amplitude at twice the ISEE 3 spin frequency (the spin period is about 3 s) which indicates that the waves are highly polarized. The mid-frequency wave amplitudes also occasionally show ripple at twice the spin frequency (e.g. near 1921 UT).

After 1919 UT, the  $B_y$  and  $B_z$  components developed quite regular oscillations with peak-to-peak amplitudes of 1 to 2 nT. Although somewhat similar and less regular, oscillations also occur in  $B_x$  and the field strength. The field oscillations have periods between 8 to 12 seconds which, in the 5 to 8 nT field, are comparable to the ion gyroperiod. Thus these magnetic oscillations might be the ion cyclotron waves which *Winske and Omidi* [1990] and *Omidi and Winske* [1992] observed in hybrid simulations of slow shocks. In the simulations escaping downstream ions interact in the upstream region with the cold incoming ions via the electromagnetic ion/ion cyclotron instability. The excited waves can be convected into the downstream region and even disrupt the shock structure, making the shock unsteady.

Figure 3b presents the high resolution measurements from the middle to top of the slow shock's magnetic ramp. At low frequencies the 56 Hz E-field amplitudes gradually diminish toward the upstream direction. The mid-frequency emissions maintain the same signal strength and temporal character throughout the ramp; note that the electron cyclotron frequency passes from below (at 1922 UT) to above (at 1926 UT) the 316 Hz channel without significantly affecting these emissions. The high frequency wave amplitudes slowly decrease, and the 1.78 kHz and 3.16 kHz channels approach background after 1925 UT. The spin ripple in these channels abruptly stops at 1924:40 UT. The emissions in the 5.62 kHz channel change character between 1923 and 1925

UT, becoming temporally more impulsive. After 1924:40 UT, the wave spectra show that the 5.62 kHz signals are narrowband electron plasma oscillations. *Feldman et al.* [1985] show that the electron density and temperature jumps occur about 1923 to 1924 UT which corresponds to the cessation of the high-frequency emissions and the onset of electron plasma oscillations at 5.62 kHz. The magnetic oscillations in all components continued during the shock ramp until 1924 UT. The peak-to-peak fluctuation amplitude is about 4 nT in  $B_y$  and  $B_z$ , about 2 nT in  $B_x$  and 1.5 nT in  $B$ . (Note the different scales in Figure 3b and the change in scale from Figure 3a.) After 1924 UT the oscillation amplitude in  $B_x$  became quite small.

The measurements from the immediate upstream region are displayed in Figure 3c. Magnetic fluctuations continue with reduced,  $< 1$  nT, amplitudes. At 1929:40 UT  $B_y$  develops a new and more regular oscillation with a period of about 10 seconds; the local ion cyclotron period is about 6 seconds. The  $B_x$  and  $B_z$  components exhibit very little variation at this time; thus, the magnetic wave is nearly linearly polarized, which is consistent with the *Winske and Omid* [1990] prediction for the electromagnetic ion/ion cyclotron instability. A few minutes after 1930 UT, (see Figure 1 of *Coroniti et al.* [1988])  $B_y$  and  $B_z$  do develop coherent and nearly equal amplitude oscillations which are probably the ion-driven right-hand magnetosonic waves discovered by *Tsurutani et al.* [1985].

In the electric field measurements, both the mid-frequency and electron plasma oscillations persist upstream. At low frequencies, impulsive emissions at 56 Hz and 100 Hz commence at 1928 UT. Interestingly, just after the first cycle of the strong  $B_y$  oscillations, the plasma emitted a strong broadband (56 Hz to 5.6 kHz) burst of electrostatic noise. *Winske and Omid* [1990] have speculated that electromagnetic ion/ion cyclotron unstable waves might nonlinearly trap ions and thus create free energy which could excite higher frequency electrostatic waves.

### *February 11, 1983 Slow Shock*

Figures 4 a,b display the high resolution magnetic field and E-field measurements from 2022 to 2030 UT for the February 11, 1983 slow shock crossing. The  $B_x$  component passes through zero at 2022:35 and remains close to zero until 2022:42 UT. At 2022:35 UT  $|B_z|$  and the field strength sharply increases from 1 nT to 5 nT. At 2023 UT  $|B_x|$  increases as  $|B|$  diminishes so that the field magnitude remains relatively constant at a plateau value of 4 nT from 2023 to 2024:30 UT. Although the magnetic field fluctuates during this interval, the oscillations do not have a clear wave-like character. Before 2023:09 UT, the E-field amplitudes are low and fairly constant in all frequency channels. At 2023:09 UT, when the  $|B_x|$  ( $|B_z|$ ) increase (decrease) is completed, the

mid-frequency amplitudes suddenly exhibit a sharp spike, and then gradually increase in amplitude and temporal variability.

Just after 2024 UT,  $|B_x|$  and the magnetic field strength increase to a second plateau value of about 10 nT. The field magnitude and components now exhibit wave-like oscillations with periods of 10 to 15 seconds and peak-to-peak amplitudes of about 4 nT in the components and 1.5 nT in the magnitude. The local ion cyclotron frequency is 6 seconds, so that the wave properties are consistent with being ion cyclotron waves. During the second magnetic plateau interval, the E-field emissions increased in intensity and temporal variability. The high frequency signals are often modulated at twice the satellite spin frequency; near 2025:50 UT, the 56 to 178 Hz channels also exhibit spin modulation.

At 2028 UT the magnetic field starts the final ramp to the upstream value. The magnetic oscillations diminish in amplitude, and disappear just after 2030 UT (not shown). During the ramp the high frequency plasma waves decrease in amplitude, and the emission drops below 10 kHz after 2028:40 UT. At this time the electron plasma frequency is about 5.6 kHz; however the high frequency signals remain broadband and there is no evidence of electron plasma oscillations. The amplitudes of the mid-frequency waves also decrease toward the upstream region.

### *Discussion*

The downstream regions of both slow shocks have very similar magnetic field and plasma wave activity. In the leading edge of the ramp the electron plasma oscillations that appear upstream abruptly cease, and are replaced by a broadband high frequency emission which is spin modulated. The mid-frequency waves are strong throughout the ramp but weaken significantly and/or disappear when  $B_x$  goes to zero downstream. Strong magnetic oscillations with frequencies below the ion cyclotron frequency occur throughout the ramp, but disappear upstream.

The slow shock simulations of *Winske and Omid* [1990] and *Omid* and *Winske* [1992] have many features which closely resemble the magnetic profiles and oscillations observed in the February 2 and 11, 1983 slow shocks. In the simulations the overall shock scale length, defined as the separation between the initial decrease in magnetic field strength to the downstream vanishing of the tangential field component, is roughly  $50 c/\omega_{pi}$  based on the upstream density. For the tail slow shocks  $50 c/\omega_{pi}$  corresponds to 3 RE. Both shocks took approximately eight minutes to go from upstream to downstream; if the shock thickness is 3 RE, this traversal time would imply a shock speed of 40 km/s. A plasma sheet thickness of 3 RE and speed of 40 km/s

are reasonable in the distant tail [Richardson and Cowley, 1985; Richardson et al., 1989]. Furthermore, the slow shocks in the tail should have significantly larger propagation angles relative to the upstream field ( $\theta = 80^\circ$  to  $85^\circ$ ) than the slow shocks studied in the simulations ( $\theta = 60^\circ$ ). Since the shock heated ions would be better confined by the higher field inclination angles, the scale length of the tail slow shocks could be considerably smaller than in the simulation shocks.

The magnetic oscillations observed in the tail slow shocks are similar to the Alfvén waves excited by the electromagnetic ion/ion instability in the simulation shocks. In both cases, the magnetic waves begin at the leading edge of the magnetic ramp and continue throughout the shock transition. The wave amplitudes in the tail shocks relative to the upstream field strength are of order  $\delta B_y/B_1 = 0.1$  to  $0.2$  whereas in the simulations the amplitudes are somewhat higher  $\delta B_y/B_1 = 0.2$  to  $0.5$ . In the nonlinear evolution of the electromagnetic ion/ion instability [Winske and Omidi, 1992], the ion fluctuation velocity in the wave field (roughly  $\delta v_y$  proportional to  $\delta B_y$ ) is eventually converted into random thermal motion by nonlinear wave breaking and phase space mixing. Hence the lower wave amplitudes observed in the tail slow shocks may imply that the wave instability may not be as effective in heating the upstream ions to the required downstream Rankine-Hugoniot temperature as in the simulation shocks.

#### 4. Wave Electric Field Polarization

For both the February 2 and 11 slow shocks the magnetic field direction and magnitude changed sufficiently slowly that meaningful electric field polarization measurements can be made. The ISEE 3 antenna is in the spin plane (the x-y plane), and six E-field measurements are obtained in one spin period. For most of the slow shock encounters, the magnetic field was predominantly in the x-y plane, so that the rotating antenna sampled both the parallel and perpendicular components of the wave electric fields. In the polarization plots displayed in Figures 5 - 8, the projection of the magnetic field on the spin plane is shown by the solid line labeled B. The radial distance from the origin is proportional to the logarithm of the electric field spectral amplitude (actually the voltage in the automatic gain control, AGC, amplifier) and the radial scale covers five decades. Each polarization plot contains two minutes or 240 measurements of the electric field. The direction of the sun (positive x) is toward the left and dusk (positive y) is toward the bottom.

#### *High Frequency Emission*

Figure 5 displays four successive polarization measurements for the 3.16 kHz E-field channel for the interval 1914 UT to 1922 UT during the February 2, 1983 slow shock traversal; during this period the high frequency emission is centered at 3.16 kHz. Between 1914 UT to 1918 UT, the spacecraft was located on the opposite side of the neutral sheet or  $B_x$  reversal from the slow shock. The peak spectral amplitudes clearly occur when the antenna is oriented more nearly parallel to the magnetic field; the ratio of the maximum parallel to perpendicular amplitudes is about 10. Between 1916 UT and 1918 UT, the satellite was very close to the center of the plasma sheet, and the magnetic field and E-field polarization were predominantly in the y direction. From 1918 UT to 1922 UT the magnetic field rotated from being along y to its dominant direction in the shock ramp along x, and the peak E-field amplitudes followed the magnetic field direction change. The bottom two panels in Figure 6 display the 3.16 kHz polarization measurements for the February 11, 1983 slow shock; once again, the peak amplitudes occur preferentially along the field and follow the changing field direction.

The high frequency emission is clearly polarized parallel to the magnetic field. Recall that this field-aligned polarization was apparent in the previous high time resolution plots as a modulation of the channel amplitudes at twice the spin frequency. In the ISEE 3 measurements of the low Mach number fast bow shock in the distant flank region, the high frequency emissions detected in the downstream region, which are spectrally similar to those in the slow shock, were also polarized parallel to the magnetic field. Thus the fast and slow shock high frequency modes may have a common origin.

### *Mid-frequency Emission*

Figure 6 presents four polarization measurement of the mid-frequency emissions obtained during the February 2, 1983 slow shock. The top (bottom) two panels show the 178 (316) Hz amplitudes which are the peak amplitude channels during the measurement interval. At 1914 UT the highest amplitudes clearly occurred when the antenna was oriented parallel to the magnetic field. From 1920 UT through 1930 UT, which corresponds to the shock ramp and near upstream region, the magnetic field is oriented nearly along the x-direction. The E-field amplitudes do not exhibit a visually apparent polarization direction, although the largest amplitudes do occur when the antenna is more nearly parallel to the magnetic field. In Figure 7 the top panels display the 178 Hz polarization measurements for the February 11, 1983 slow shock. The downstream (2022 UT) mid-frequency emissions are polarized along the field whereas the signals from the plateau in the shock ramp (2026 UT) do not have an apparent polarization; the polarization measurements in the steep shock ramp (not shown) are almost identical to those at 2026 UT.

The clear detection of a wave polarization using channel amplitudes, however, can be obscured if the signal strength has very large and rapidly fluctuating changes. The mid-frequency emissions are highly impulsive with peak-to-valley amplitude changes of  $10^2$  to  $10^3$  in a few measurement cycles. Suppose that the mid-frequency waves are actually polarized with the electric field exactly along the magnetic field. If a very high peak amplitude occurs when the antenna is nearly perpendicular to the magnetic field, its projection onto the antenna direction can still result in an electric field amplitude measurement which significantly exceeds the average value. If the next impulsive emission has a lower amplitude, but the antenna is now oriented along the magnetic field, the perpendicular and parallel emissions can appear to have the same amplitude, and the signal will appear to be unpolarized. Since the above polarization diagrams display the logarithm of the amplitude, the polarization of the impulsive signals is even more difficult to visually discern.

Figure 8 displays the polarization measurements of the mid-frequency emissions (178 and 316 Hz), the high frequency emission (3.16 kHz), and electron plasma oscillations (5.6 kHz) at the start of the shock ramp (1920 UT) and the near upstream region (1922 UT) for the February 2, 1983 slow shock. Superposed on the amplitude measurements, we have drawn two curves. The inner circle corresponds to the average electric field amplitude for the two minute interval over which the 240 sample measurements were obtained. The outer curve was constructed by first taking the largest E-field amplitude  $E_p(\phi_p)$  (or voltage  $V_p(\phi_p)$ ) measured during the two minute interval at angle  $\phi_p$  between the antenna and magnetic field. We then project it back to the magnetic field direction as  $E_p(\phi_p = 0) = E_p(\phi_p)/\cos(\phi_p)$  ( $V_p(\phi_p = 0) = V_p(\phi_p) + (1/b)\ln(1/\cos(\phi_p))$ ) where  $b$  is a calibration constant. The outer curve is then given by the function  $V(\phi) = V_p(\phi = 0) - (1/b)\ln(1/\cos(\phi))$ . If the wave emission is polarized parallel to the magnetic field, there should be no E-field (voltage) values outside of the curve  $V(\phi)$  at any  $\phi$ .

First consider the 3.16 kHz polarization diagram at 1920 UT in Figure 8 (which is also displayed in Figure 5). The region between the peak  $V(\phi)$  and average curves is fairly uniformly populated even though, from Figure 5, the high frequency emission is clearly polarized along the magnetic field. Although there are many measurements with  $\phi$  near  $90^\circ$ , only one value lies just slightly outside the  $V(\phi)$  curve. If the wave electric fields were not strongly aligned with the magnetic field, we should observe some signals near  $\phi = 90^\circ$  with amplitudes exceeding  $V(\phi)$ . Next consider the 5.6 kHz electron plasma oscillations at 1928 UT. It is commonly thought that plasma oscillations are parallel polarized since the most likely excitation sources are field-aligned electron beams. The 5.62 kHz polarization diagram, however, does not give a strong visual impression that these waves are parallel polarized. The plasma oscillations are highly impulsive signals with

large peak-to-valley ratios, thus making a polarization determination difficult. The only indication that the plasma oscillations are parallel polarized is the absence of large amplitude signals outside the  $V(\phi)$  curve near  $\phi = 90^\circ$ .

Finally consider the mid-frequency polarization diagrams. Visually these diagrams are not significantly different than the 5.62 kHz plasma oscillation case; there is a definite absence of high amplitude signals near  $90^\circ$ . Thus, although the polarization diagrams do not prove that the mid-frequency waves are polarized along the magnetic field, the polarization measurements are consistent with parallel polarization given the highly impulsive nature of the emissions.

## 5. Discussion

The slow shocks in the distant geomagnetic tail exhibit a coherent internal structure in both their magnetic field oscillations and plasma wave properties. Within the shock ramp, the magnetic waves have frequencies which are comparable (0.5 to 1.0) to the local ion cyclotron frequency and fluctuation amplitudes  $\delta B/B$  approximately 0.1 to 0.2 relative to the upstream field strength. The fluctuation amplitude in the transverse field components is typically a factor two larger than in the field magnitude. The observed wave properties are generally consistent with the simulation predictions that electromagnetic ion/ion cyclotron modes are excited by the beam-interaction between the upstream cold ions and the shock-heated, escaping downstream ions [Winske and Omid, 1990; Omid and Winske, 1992]. The observed wave amplitudes, however, are somewhat smaller than in the simulations.

The magnetic ramps in simulation slow shocks are typically of order  $50 c/\omega_{pi}$ , which corresponds to roughly  $3 R_E$  in the distant tail. A single satellite, of course, cannot resolve space-time ambiguities, so we cannot determine the observed shock thickness. However, we can make the following estimate of the thickness based on the observed magnetic wave amplitudes. If we view the shock interaction in the deHoffman-Teller frame, the upstream ions flow along the magnetic field with velocity  $v_{//} = C_A$ , the upstream Alfvén speed, assuming oblique switch-off shock conditions. Since the electric field vanishes in the deHoffman-Teller frame, the upstream ions have all the kinetic energy needed to produce the downstream temperature  $T_2 = (\gamma - 1)m_i C_A^2 / 2\gamma$  where  $\gamma$  is the adiabatic index. As the upstream ions enter the shock ramp and excite the ion cyclotron waves, they will be scattered essentially in pitch-angle to form the downstream heated distributions. For an approximate pitch-angle diffusion coefficient  $D_{\alpha\alpha} = \Omega_i (\delta B/B)^2$  [Kennel and Petschek, 1966], we can write a phenomenological heating equation for the ions.

$$v_{||}(\partial T/\partial s) = D\alpha\alpha [(\gamma-1)m_i C_{A1}^2/2\gamma - T]$$

where  $s$  is the distance along a field-line. Very roughly an upstream ion must travel a parallel distance  $\Delta s \approx C_{A1}/D\alpha\alpha \approx c/\omega_{pi}(B/\delta B)^2 \approx 25 - 100 c/\omega_{pi}$ . For switch-off shocks the shock thickness,  $\lambda$ , is roughly  $\lambda \approx (B_2/B_1)\Delta s \approx 1/4\Delta s \approx 8 - 25 c/\omega_{pi} \approx 0.5 - 1.5 R_E$  for the two February shocks. Given the very approximate nature of this estimate, the thicknesses of the tail slow shocks are probably somewhat smaller, but still comparable to the ramp thicknesses in the slow shock simulations.

The plasma waves consist of distinct mid-frequency and high frequency emissions. Within the shock ramp, the high frequency mode occurs between the maximum Doppler shift frequency and the local electron plasma frequency, has a quite low amplitude, and is strongly polarized with the electric field parallel to the magnetic field. At the top of the shock ramp, the broadband high frequency mode disappears, and is replaced by higher amplitude, impulsive narrowband electron plasma oscillations. The mid-frequency waves have a clear, fairly narrowband, spectral peak, which persists from upstream of the ramp through the shock transition. For one slow shock the peak frequency at the upstream edge was close to the electron cyclotron frequency but above the ion plasma frequency; for the other shock the peak frequency was unchanged even though the field strength was two times higher. The frequency of the spectral peak decreases through the ramp, and becomes comparable to both the downstream electron cyclotron and ion plasma frequencies. Thus the peak frequency does not appear to have any obvious relation to either the magnetic field strength ( $f_c$ ) or the plasma density ( $f_{pi}$ ). In addition, the peak frequency is anti-correlated with the maximum Doppler shift frequency, which increases from upstream to downstream. The mid-frequency emissions are highly impulsive which renders difficult a clear determination of their electric field polarization. The only firm conclusion that we can draw is that the waves are not strongly polarized perpendicular to the field direction. The polarization distribution could be consistent with parallel polarization, but could also be compatible with a broad angular spread about the field direction.

The high frequency emission has not previously been identified as a distinct spectral component in either the broadband electrostatic noise in the near Earth plasma sheet [Gurnett *et al.*, 1976] or the plasma sheet and slow shock waves in the distant tail [Scarf *et al.*, 1984; Coroniti *et al.*, 1990]. However, these emissions have essentially identical spectral and polarization properties to a weak high frequency wave which occurs downstream of the low Mach number flank bow shocks [Coroniti *et al.*, 1993]. Although unaware of the high frequency emission being a distinct mode, Onsager *et al.* [1989] have suggested that waves between the ion and electron plasma frequencies

could be excited by very cold electron beams with speeds near or below the electron thermal speed. Alternatively *Coroniti et al.* [1993] proposed that discontinuities in the electron distribution function integrated over perpendicular velocities could support a non-standard, but beam-like wave mode which can be unstable if the distribution function increases across the discontinuity.

The strong similarity between the fast and slow shock high frequency emissions certainly suggests that their excitation mechanisms are similar. Furthermore, the slow shock wave observations lend support to these emissions being of electron origin. The emissions persist and follow the local magnetic field direction through the downstream region. Since the ion Larmor radius in the downstream field is large (of order  $10^8$  cm), the ion distribution should be isotropic and not sensitive to the local field direction. Thus, the ions are unlikely to contain the free energy which produces parallel polarized waves, whereas the electrons will remain magnetized, and a potential free energy source.

As for fast shocks, the electrostatic potential increases across slow shocks [*Schwartz et al.*, 1987]. Thus in slow shocks the upstream electrons are accelerated along the field by both the potential electric field and magnetic gradient force, which in the downstream distribution creates a velocity space separatrix between the trapped downstream electrons and the accelerated upstream electrons. *Feldman et al.* [1985] showed cuts of the downstream electron distribution function along zero perpendicular velocity which contained evidence for the separatrix, and perhaps a void at low parallel speeds. Since the distribution function is unlikely to always match smoothly at the separatrix, the non-standard, beam-like modes suggested by *Coroniti et al.* [1993] could exist in the downstream region of slow shocks and account for the observed high frequency emissions.

The origin of the mid-frequency emissions remains unclear. Since these modes are observed both in the upstream and ramp regions of the slow shock, the hole mode explanation of *Coroniti and Ashour-Abdalla* [1989] is probably not correct; in their model the hole at low electron energies occurred only upstream of the potential jump. The downstream electron distribution reported by *Feldman et al.* [1985] apparently has a hole at low energies; however, the distribution should be symmetric in parallel velocity so that no non-standard hole-type mode would occur. The mid-frequency waves fall in the frequency range of the broadband electrostatic noise found in the near Earth plasma sheet [*Gurnett et al.*, 1976], and thus could be generated by free energy in the ion distribution, but whether or not parallel cold ion beams [*Grabbe and Eastman*, 1984], perpendicular cold ion rings [*Huba et al.*, 1992], or hot ion beams [*Schrifer and Ashour-Abdalla*, 1987] exist in slow shocks cannot be determined with the ISEE 3 plasma instrument complement. However, the essential difficulty with all these instabilities is that, in order to obtain a solution to the dispersion

relation, the thermal speed of all ion components must be much less than the ion acoustic speed based on the electron temperature. Since  $T_e$  is almost always comparable to or less than  $T_i$  in the magnetosphere and magnetotail, the cold ion temperature constraint is very difficult to satisfy.

Recently *Onsager et al.* [1993] presented ISEE 1 and 2 observations of the plasma distributions and wave emissions in the near Earth plasma sheet boundary layer. They found, as did *Parks et al.* [1984], that the boundary layer has an outer region in which the electron distribution has enhanced fluxes and velocity space fine structure at energies above the thermal energy but the ion fluxes remained below the plasma instrument threshold, as in the lobes, and exhibited no evidence for field-aligned ion beams. The electron boundary layer contained intense wave emissions with a falling power spectrum from below the ion plasma frequency up to the electron plasma frequency; a deep spectral minimum occurred at the electron cyclotron frequency and a strong peak was positioned near the electron plasma frequency. When the spacecraft entered the ion boundary layer, the wave spectrum became a relatively featureless falling power law from low to high frequencies. *Onsager et al.* [1993] argue that boundary layer electrons alone can generate a broadband plasma wave spectrum at mid-frequencies without the necessity of involving ion beams; ion beams may only contribute to the low frequency portion of the spectrums.

The details of the electron region spectrum shown by *Onsager et al.* [1993] differ from both the upstream and shock layer spectra for the February slow shocks; instead of the slow shock's clear mid-frequency spectral peak, the electron boundary layer emissions have only flattening of the spectrum. Never the less, *Onsager et al.*'s inference that broadband emissions can be generated by electrons alone may be relevant to the slow shock waves. We argued above that the high frequency waves are probably excited by electrons, perhaps by discontinuities in the downstream distribution function induced by the slow shock potential. Since the mid-frequency spectral peak is anti-correlated with the maximum Doppler shift frequency, these emissions either have long wavelengths ( $k\lambda_D < 1/10 - 1/20$ ) to avoid Doppler shifting, or are not coupled to the flowing ion distribution, i.e., their dielectric function depends only on the electron distribution which implies a high phase speed. The phase speed can be expressed as

$$\omega/ka_e = (f/f_{pe})(2^{1/2}k\lambda_D)^{-1}$$

If we take  $k\lambda_D = 0.1$  to avoid Doppler shifting by the high downstream flow, the mid-frequency spectral peak would have phase speeds in the range  $\omega/ka_e = 0.1 - 0.2$ , which is only 1.5 to 3.0 times greater than the downstream ion thermal speed. Thus, unless  $k\lambda_D \ll 0.1$ , the mid-

frequency modes would appear to have phase velocities which couple to the ions, and render the absence of Doppler shifting even more mysterious.

Acknowledgments. The work at TRW was supported by NASA Contracts NAS5-31827 (with NASA Headquarters) and NASW-4749 (with GSFC). The work at California Institute of Technology, Jet Propulsion Laboratory was supported by contract with NASA.

#### References

Anderson, R. R., C. C. Harvey, M. M. Hoppe, B. T. Tsurutani, T. E. Eastman, and J. Etcheto, Plasma waves near the magnetopause, *J. Geophys. Res.*, *87*, 2087, 1982.

Coroniti, F. V., F. L. Scarf, C. F. Kennel, B. T. Tsurutani, and E. J. Smith, A search for lower hybrid drift turbulence in slow shocks, *J. Geophys. Res.*, *93*, 2553, 1988.

Coroniti, F. V., and M. Ashour-Abdalla, Electron velocity space hole modes and narrowband electrostatic noise in the distant tail, *Geophys. Res. Lett.*, *16*, 747, 1989.

Coroniti, F. V., E. W. Greenstadt, B. T. Tsurutani, E. J. Smith, R. D. Zwickl, and J. T. Gosling, Plasma waves in the distant geomagnetic tail: ISEE 3, *J. Geophys. Res.*, *95*, 20,977, 1990.

Coroniti, F. V., E. W. Greenstadt, S. L. Moses, E. J. Smith, and B. T. Tsurutani, Plasma waves downstream of weak collisionless shocks, *J. Geophys. Res.*, *in press*, 1993.

Feldman, W. C., S. J. Schwartz, S. J. Bame, D. N. Baker, J. Birn, J. T. Gosling, E. W. Hones, Jr., D. J. McComas, J. A. Slavin, E. J. Smith, and R. D. Zwickl, Evidence for slow-mode shocks in the deep geomagnetic tail, *Geophys. Res. Lett.*, *11*, 599, 1984.

Feldman, W. C., D. N. Baker, S. J. Bame, J. Birn, J. T. Gosling, E. W. Hones, Jr., and S. J. Schwartz, Slow-mode shocks: A semipermanent feature of the distant geomagnetic tail, *J. Geophys. Res.*, *90*, 233, 1985.

Gallagher, D. L., Short-wavelength electrostatic waves in the Earth's magnetosheath, *J. Geophys. Res.*, *90*, 1435, 1985.

Grabbe, C. L., and T. E. Eastman, Generation of broadband electrostatic waves in the magnetotail, *J. Geophys. Res.*, *89*, 3865, 1984.

Gurnett, D. A., Plasma waves and instabilities, in *Collisionless Shocks in the Heliosphere Review of Current Research, Geophys. Mono. Ser.*, vol. 35, ed. by B. T. Tsurutani and R. G. Stone, 207-224, AGU, Washington DC, 1985.

Gurnett, D. A., L. A. Frank, and R. P. Lepping, Plasma waves in the distant magnetotail, *J. Geophys. Res.*, *81*, 6059, 1976.

Huba, J. D., J. Chen, and R. R. Anderson, Electrostatic turbulence in the Earth's central plasma sheet produced by multiple ring ion distributions, *J. Geophys. Res.*, *97*, 1533, 1992.

Kennel, C. F., and H. E. Petschek, Limit on stably trapped particle fluxes, *J. Geophys. Res.*, *71*, 1, 1966.

Omidi, N. and D. Winske, Kinetic structure of slow shocks: Effects of the electromagnetic ion/ion cyclotron instability, *J. Geophys. Res.*, *97*, 14,801, 1992.

Onsager, T. G., R. H. Holzworth, H. C. Koons, O. H. Bauer, D. A. Gurnett, R. R. Anderson, H. Luhr, and C. W. Carlson, High frequency electrostatic waves near Earth's bow shock, *J. Geophys. Res.*, *94*, 13,397, 1989.

Onsager, T. G., M. F. Thomsen, R. C. Elphic, J. T. Gosling, R. R. Anderson, and G. Kettmann, Electron generation of electrostatic waves in the plasma sheet boundary layer, *J. Geophys. Res.*, *98*, 15,509, 1993.

Parks, G. K., M. McCarthy, R. J. Fitzenreither, J. Etcheto, K. A. Anderson, R. R. Anderson, T. E. Eastman, L. A. Frank, D. A. Gurnett, C. Huang, R. P. Lin, A. T. Y. Lui, K. W. Ogilvie, A. Pederson, H. Reme, and D. J. Williams, Particle and field characteristics of the high-latitude plasma sheet boundary layer, *J. Geophys. Res.*, *89*, 8885, 1984.

Richardson, I. G., S. W. H. Cowley, Plasmoid-associated energetic ion bursts in the deep geomagnetic tail: Properties of the boundary layer, *J. Geophys. Res.*, *90*, 12,133, 1985.

Richardson, I. G., C. J. Owen, S. W. H. Cowley, A. B. Galvin, T. R. Sanderson, M. Scholer, J. A. Slavin, and R. D. Zwickl, ISEE 3 observations during the CDAW-8 intervals: Case studies of the distant geomagnetic tail covering a wide range of geomagnetic activity, *J. Geophys. Res.*, *94*, 15,189, 1989.

Rodriquez, P., Magnetosheath electrostatic turbulence, *J. Geophys. Res.*, *84*, 917, 1979.

Scarf, F. L., F. V. Coroniti, C. F. Kennel, E. J. Smith, J. A. Slavin, B. T. Tsurutani, S. J. Bame, and W. C. Feldman, Plasma wave spectra near slow mode shocks in the distant magnetotail, *Geophys. Res. Lett.*, *11*, 1050, 1984.

Schriver, D., and M. Ashour-Abdalla, Generation of high frequency broadband electrostatic noise; The role of cold electrons, *J. Geophys. Res.*, *92*, 5807, 1987.

Schwartz, S. J., M. F. Thomsen, W. C. Feldman, and F. J. Douglas, Electron dynamics and potential jump across slow mode shocks, *J. Geophys. Res.*, *92*, 3165, 1987.

Tsurutani, B. T., I. G. Richardson, R. M. Thorne, W. Butler, E. J. Smith, S. W. H. Cowley, S. P. Gary, S. I. Akasofu, and R. D. Zwickl, Observations of the right-hand resonant ion beam instability in the distant plasma sheet boundary layer, *J. Geophys. Res.*, *90*, 12,159, 1985.

Winske, D., and N. Omidi, Electromagnetic ion/ion cyclotron instability at slow shocks, *Geophys. Res. Lett.*, *17*, 2297, 1990.

Winske, D., and N. Omidi, Electromagnetic ion/ion instability: Theory and simulations, *J. Geophys. Res.*, *97*, 14,779, 1992.

## Figure Captions

Figure 1. Selected electric field spectral amplitudes (Volts/m-Hz<sup>1/2</sup>) from 17.8 Hz to 100 kHz for the February 2, 1983 slow shock. The lower (upper) curves in each spectrum is the 30 second average (peak in 30 second interval) spectral amplitude in each frequency channel. The mid-frequency and high frequency emissions have clearly separated peaks in the 1920:50 UT spectrum.

Figure 2. Selected electric field spectral amplitudes for the February 11, 1983 slow shock.

Figures 3 a,b,c. High time resolution measurements for the February 2, 1983 slow shock. The top four panels display the vector components and magnitude of the magnetic field at 6 vectors/second resolution. Note the change in scale from Figure 3a to 3b and c. The bottom panels display the wave electric field measurements for the 56 Hz to 10 kHz channels; the scale is logarithmic and the 10<sup>-7</sup> V/m-Hz<sup>1/2</sup> and 10<sup>-4</sup> V/m-Hz<sup>1/2</sup> levels are indicated.

Figures 4 a,b. High time resolution measurements for the February 11, 1983 slow shock in the same format as Figure 3. Note the change in scale on the magnetic field magnitude panel from Figure 4 a to b.

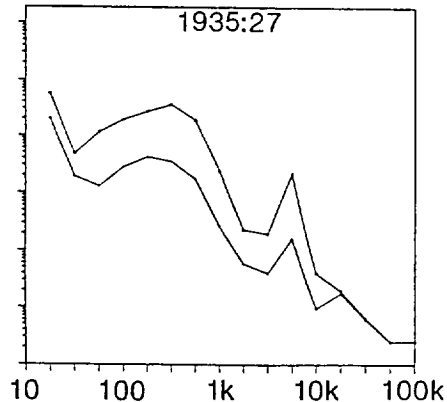
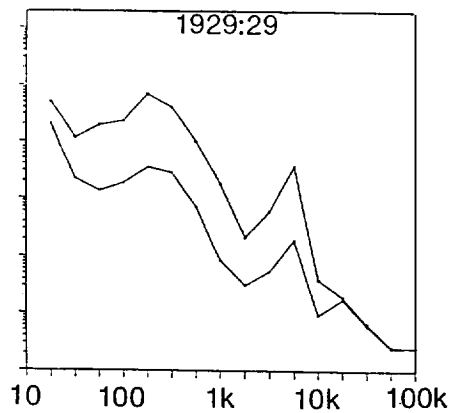
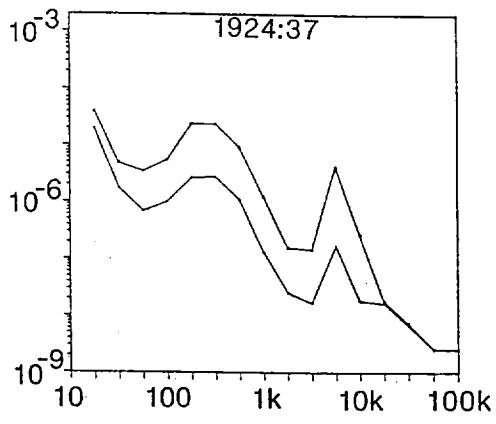
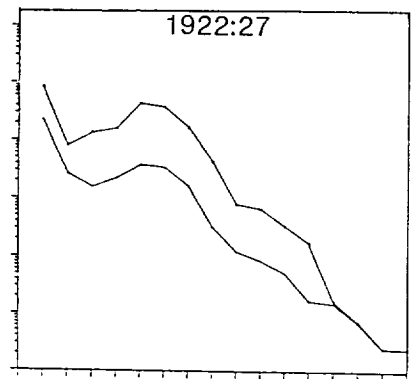
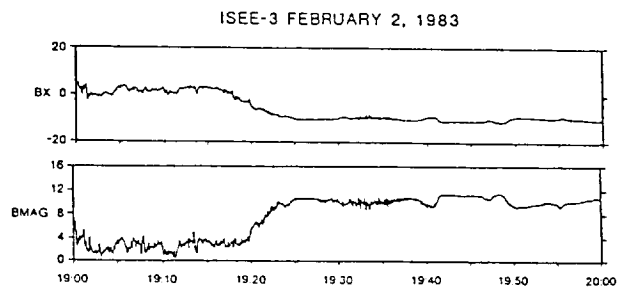
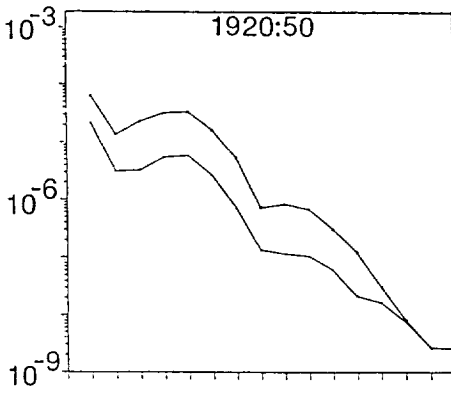
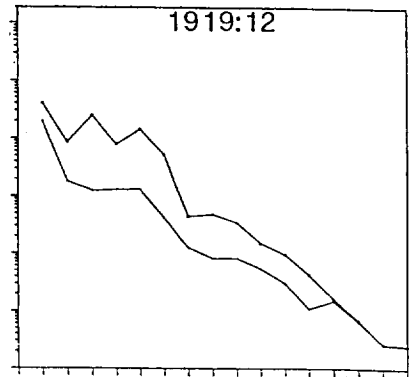
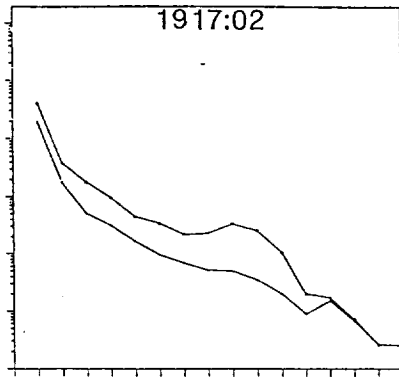
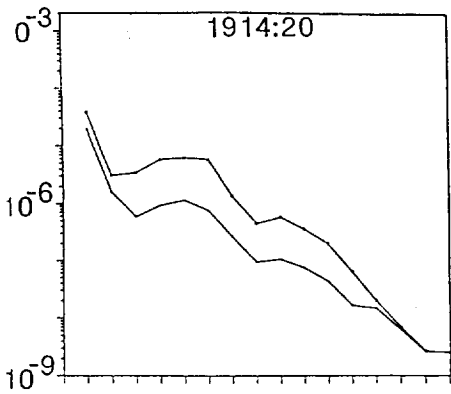
Figure 5. The electric field polarization of the high frequency (3.16 kHz) emission during the February 2, 1983 slow shock. The radial scale is proportional to the logarithm (base 10) of the electric field spectral amplitude with a range of five decades. The sun is toward the left and dusk is toward the bottom of each diagram. Each polarization diagram contains two minutes of 240 electric field measurements. The ISEE 3 single-axis antenna is in the ecliptic plane and rotates about the ecliptic pole once every 3 seconds. The line labeled B is the ecliptic projection of the magnetic field; the magnetic field vector was essentially in the ecliptic plane throughout this interval.

Figure 6. The electric field polarization of the mid-frequency emissions for the February 2, 1983 slow shock. The format is the same as in Figure 5.

Figure 7. The electric field polarization of the mid-frequency (top) and high-frequency (bottom) emissions for the February 11, 1983 slow shock.

Figure 8. The electric field polarization of the mid-frequency (178 Hz and 316 Hz), high frequency (3.16 kHz), and electron plasma oscillations (5.62 kHz) in the ramp (1920 UT) and upstream (1928 UT) regions of the February 2, 1983 slow shock. The inner circle represents the

average electric field spectral amplitude in the indicated frequency channel for the two minute interval. The outer curve assumes that the largest electric field amplitude measured during the two minute interval was produced by a parallel polarized signal, and represents the projection of that amplitude about the magnetic field direction in a dipole pattern. If the emissions are actually parallel polarized, no signals should occur outside this dipole projection curve.



f(Hz)

Fig. 1

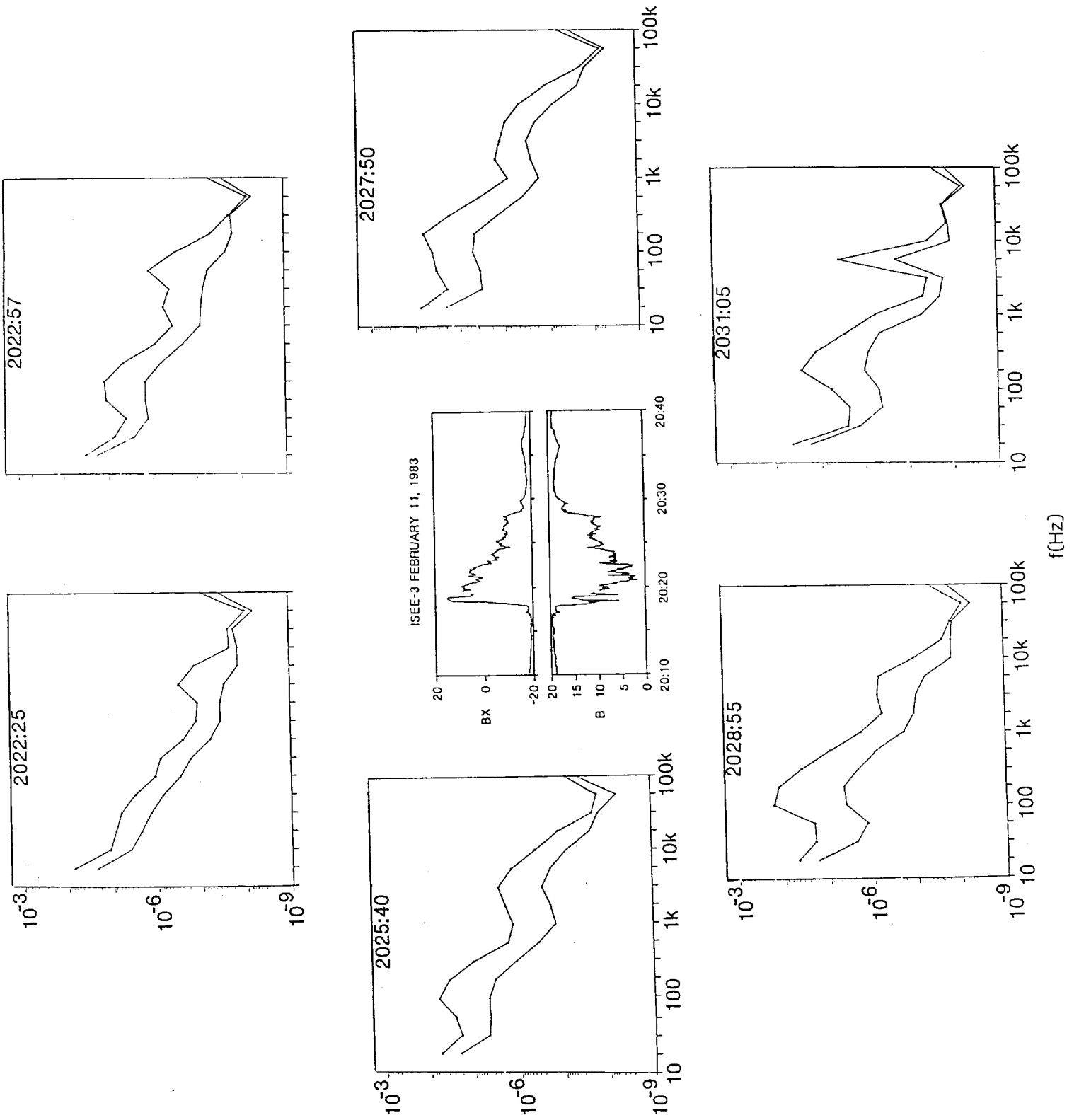


FIG 2

ISEE 3 February 2, 1983

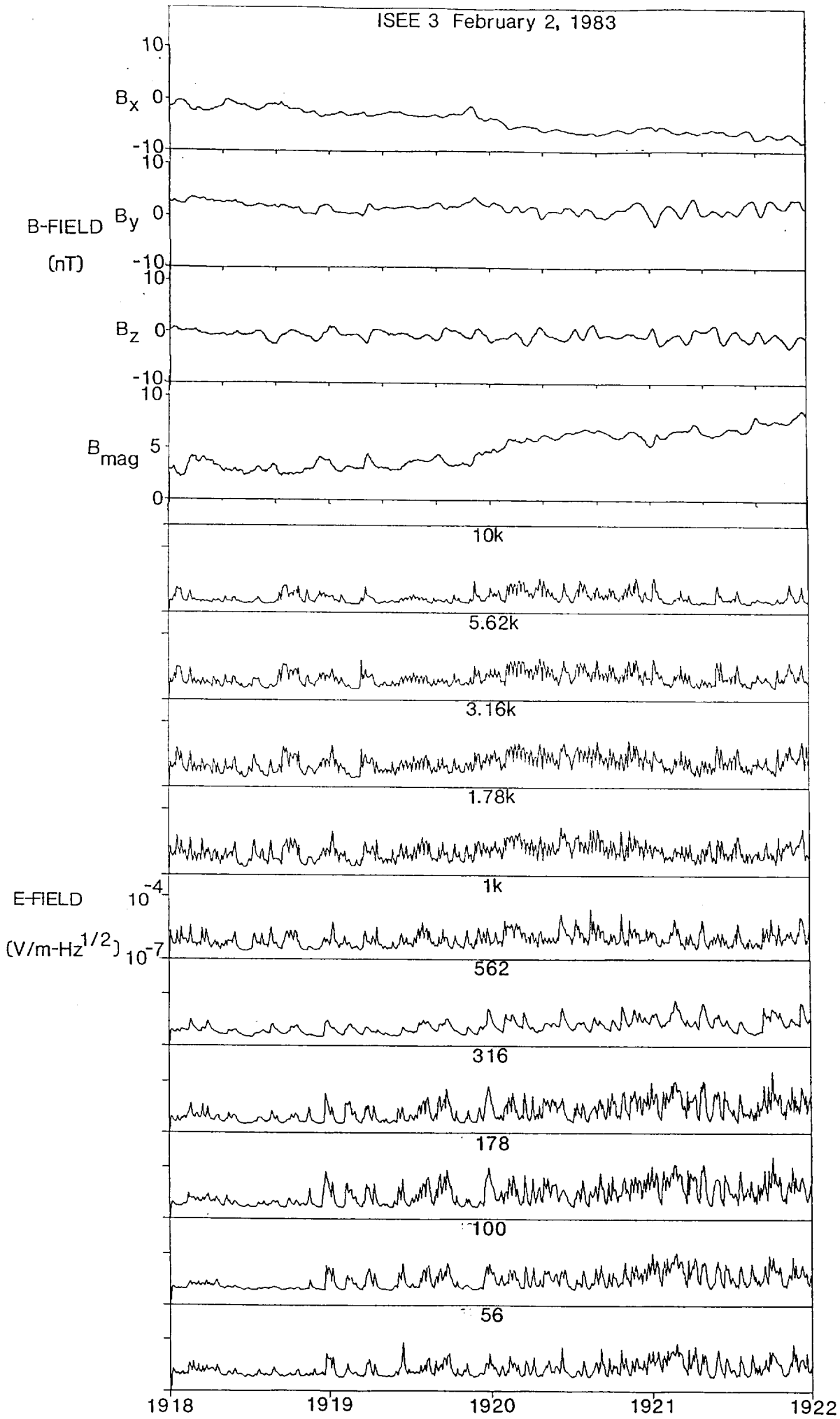


FIG 3a

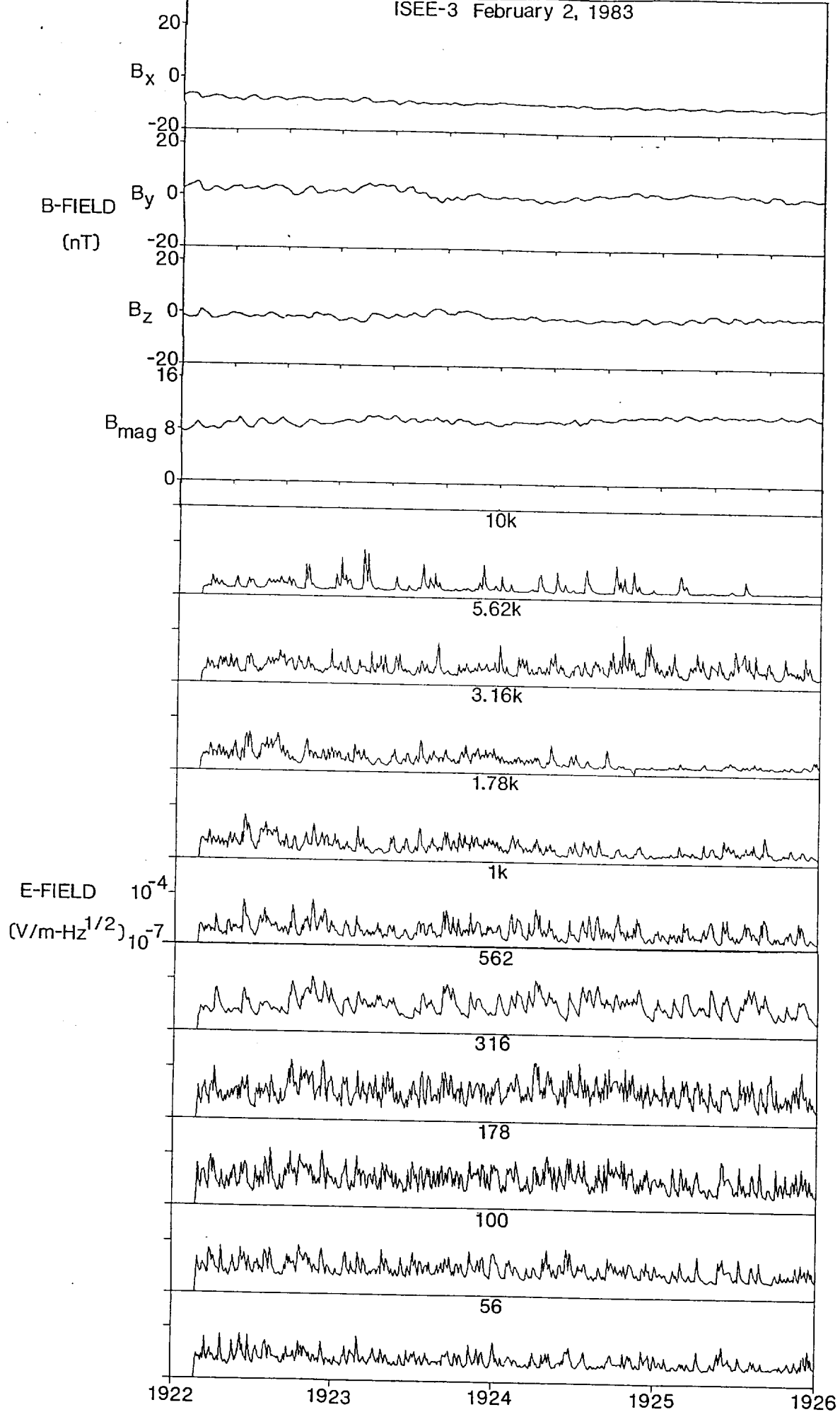


FIG 3b

ISEE 3 February 2, 1983

20

$B_x$  0

-20

20

B-FIELD

$B_y$  0

(nT)

-20

20

$B_z$  0

-20

16

$B_{mag}$  8

0

10k

5.62k

3.16k

1.78k

1k

E-FIELD

$10^{-4}$

( $V/m-Hz^{1/2}$ )

$10^{-7}$

562

316

178

100

56

1926

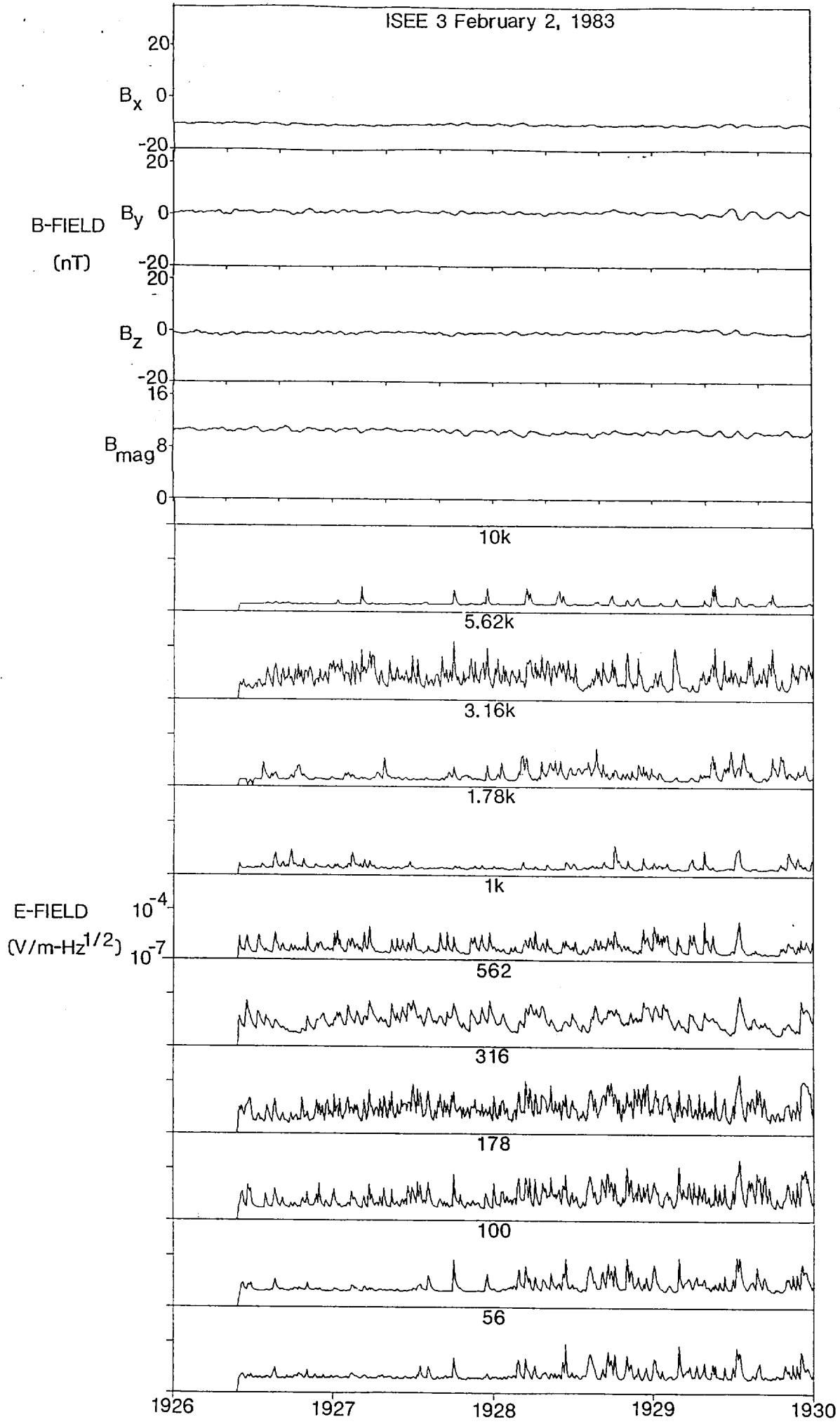
1927

1928

1929

1930

FIG 3c.



ISEE 3 February 11, 1983

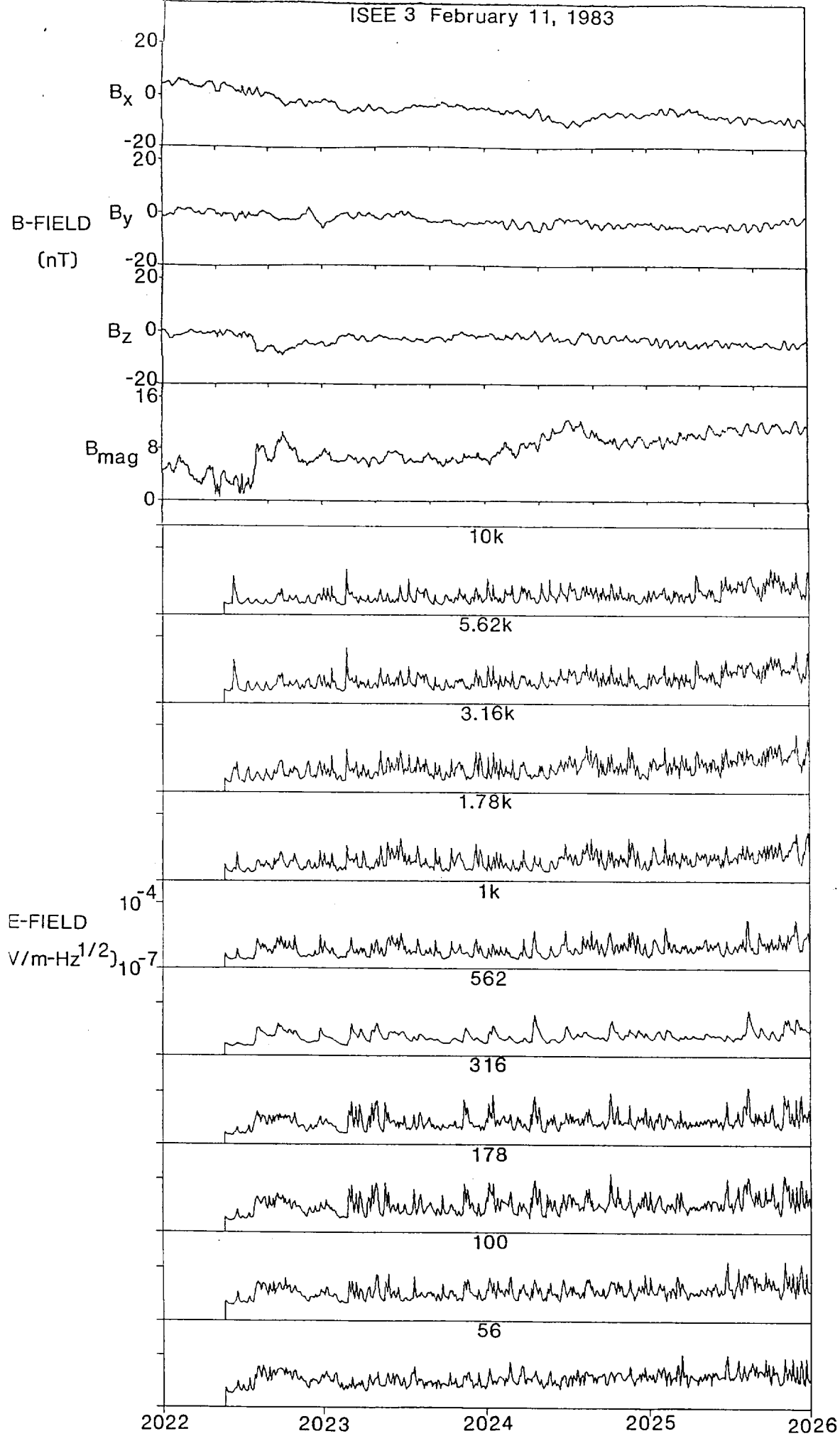


FIG 4a

ISEE 3 February 11, 1983

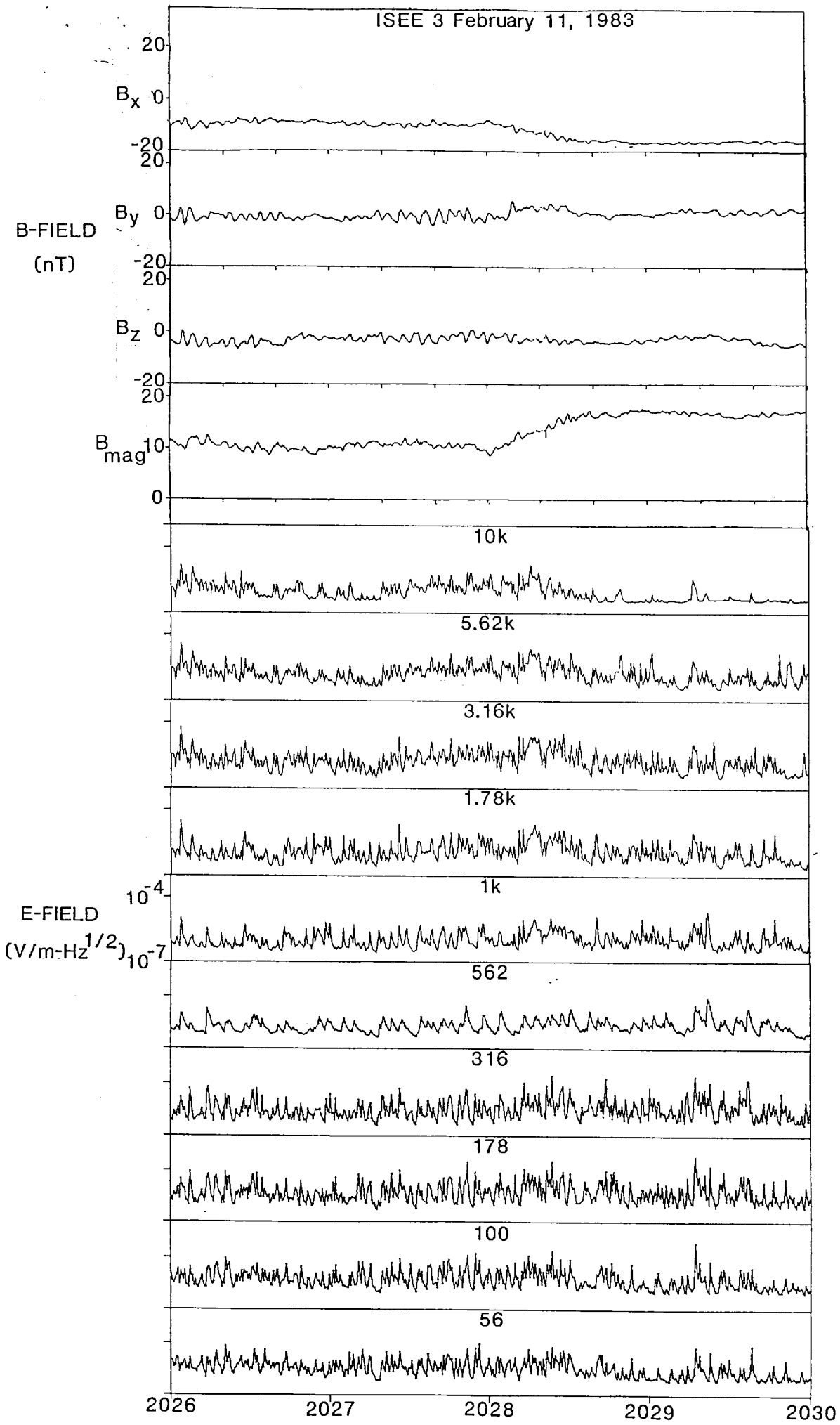
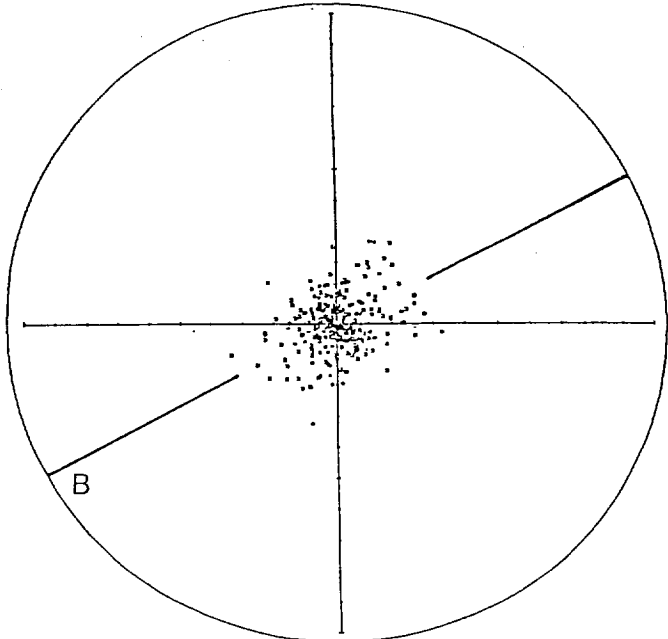
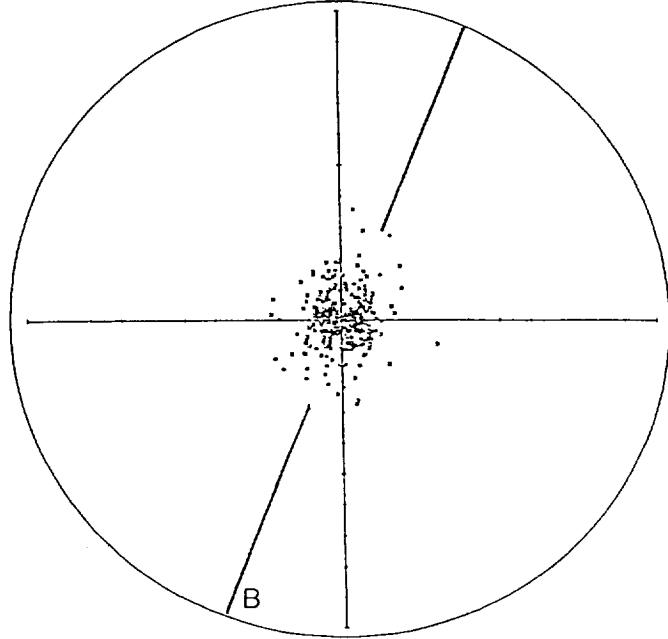


Fig 4b

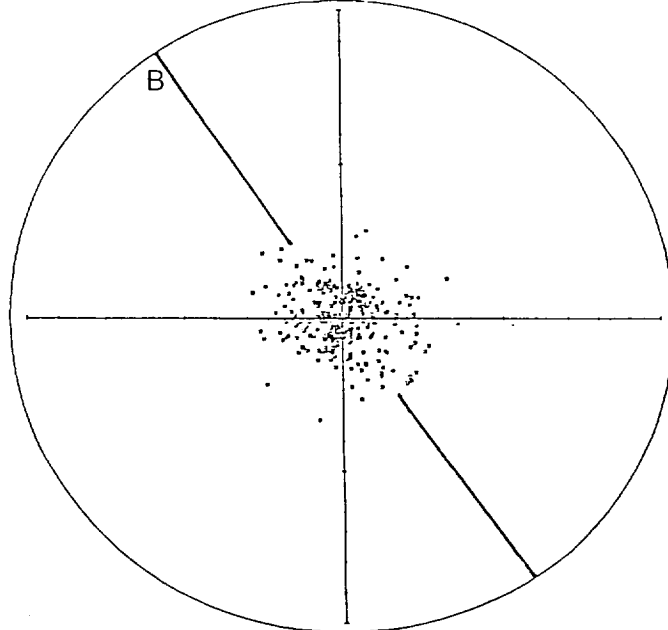
1914-1916



1916-1918

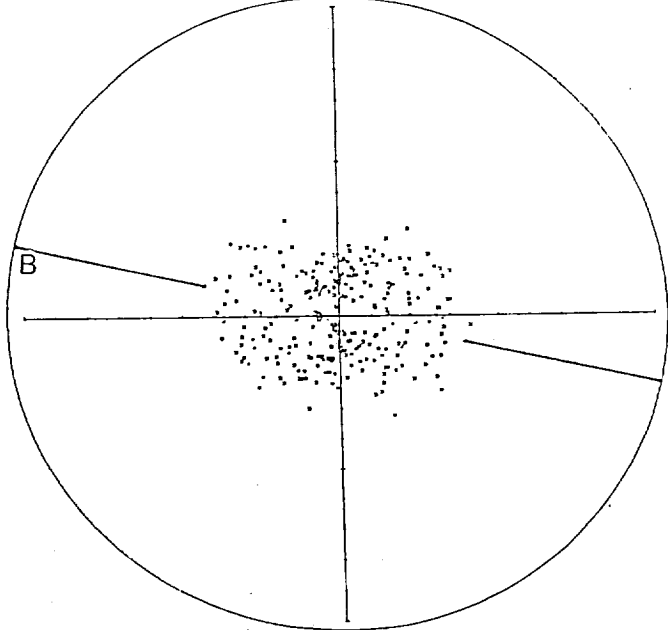


1918-1920

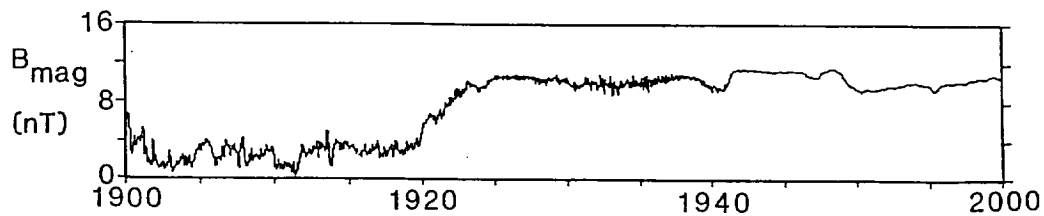


3.16 kHz

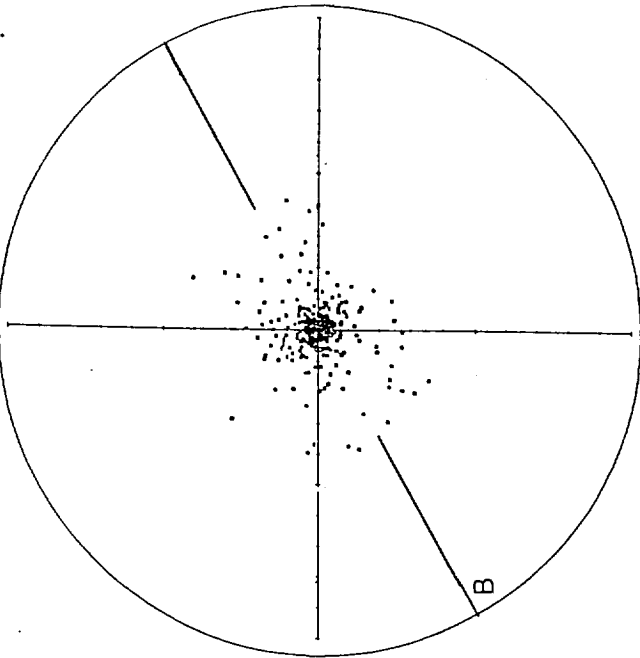
1920-1922



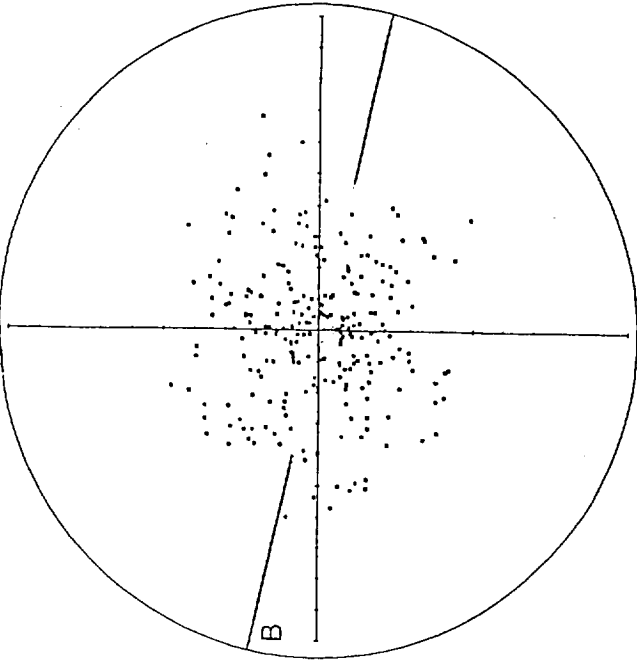
ISEE 3 February 2, 1983



1914-1916

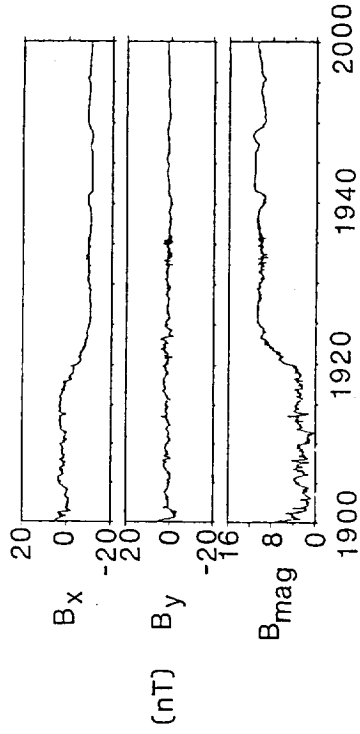


1920-1922

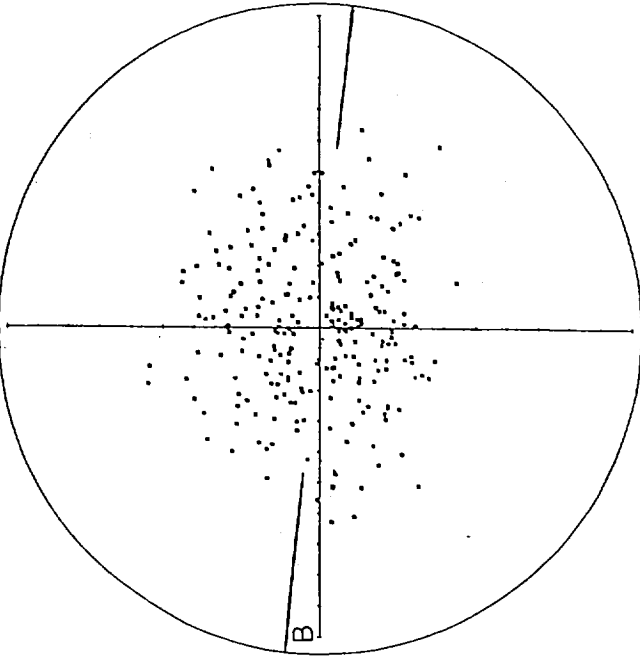


178 Hz

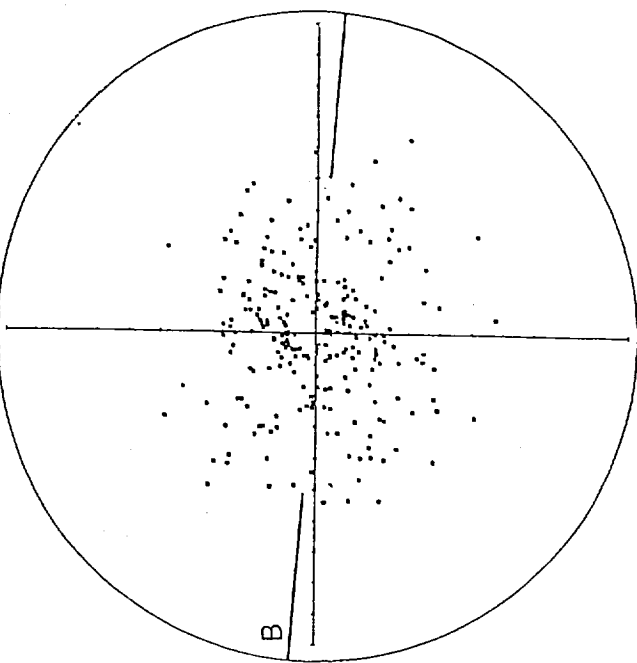
ISEE 3 February 2, 1983



1924-1926

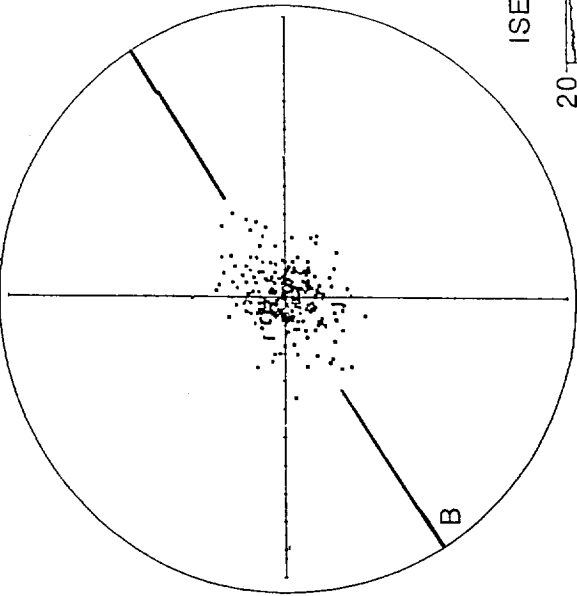


1928-1930



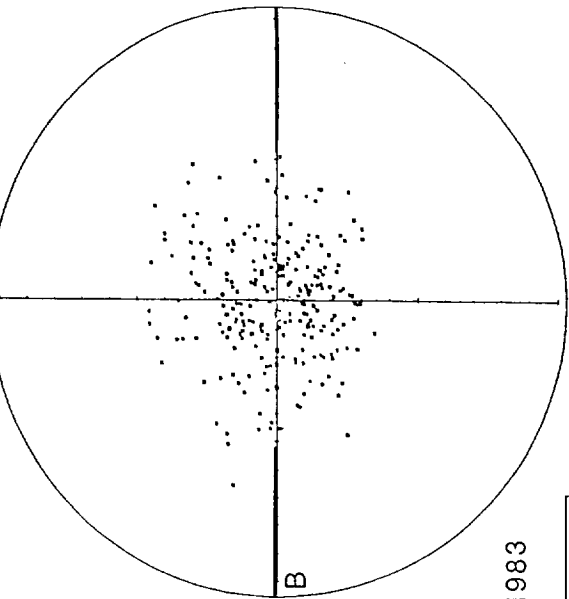
316 Hz

2022-2024

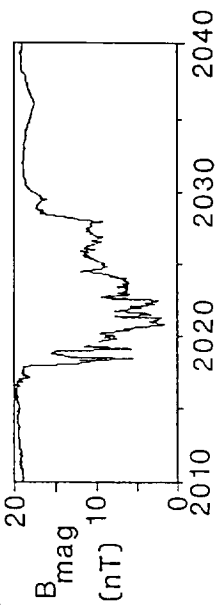


178 Hz

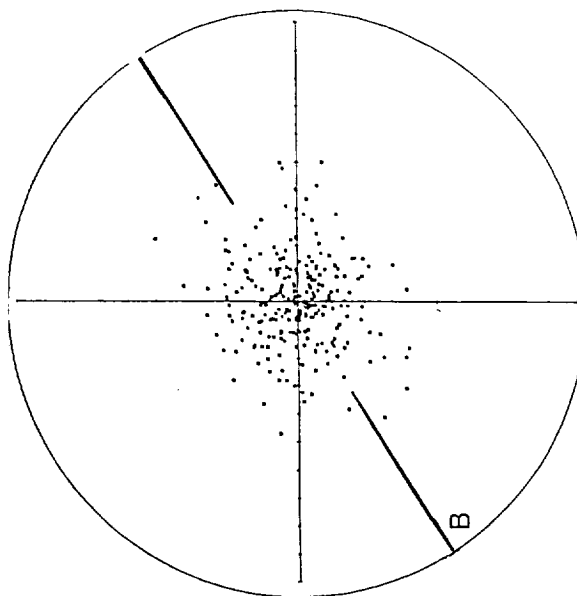
2026-2028

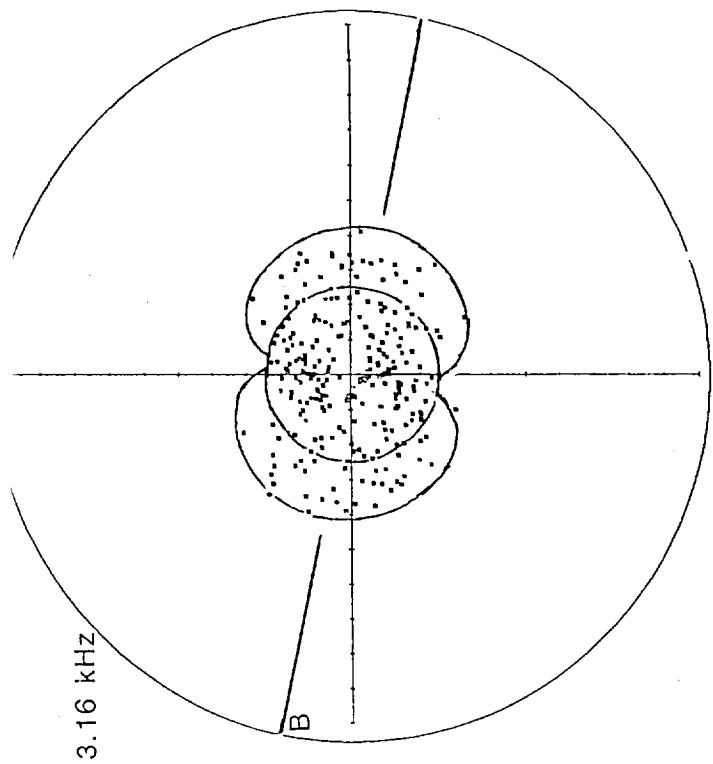
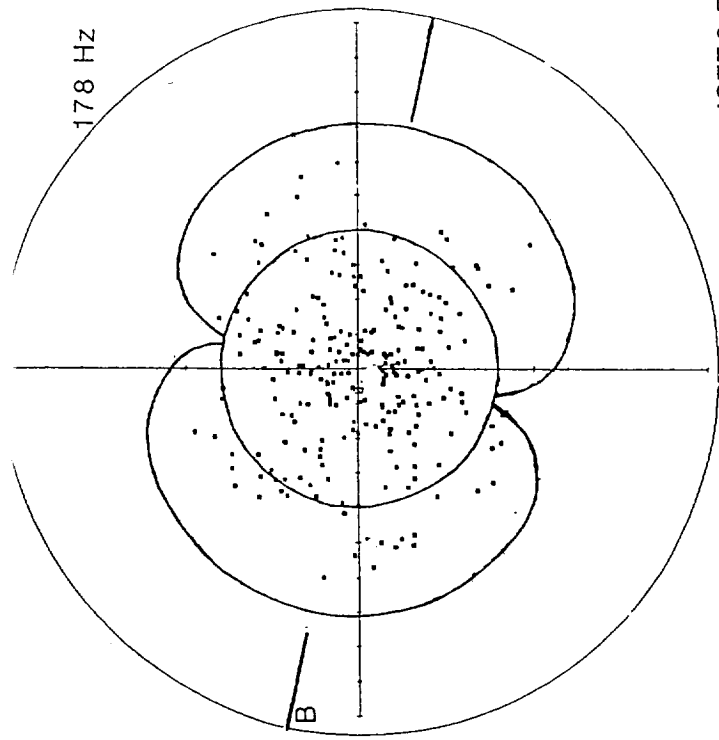


ISEE 3 February 11, 1983



3.16 kHz





ISEE3 February 2, 1983

